NATIONAL ADVISORY COMMITTEE FOR AERONAUTICS

TECHNICAL NOTE 3079

THE HYDRODYNAMIC CHARACTERISTICS OF MODIFIED RECTANGULAR FLAT PLATES HAVING ASPECT RATIOS OF 1.00 AND 0.25 AND OPERATING NEAR A FREE WATER SURFACE

By Kenneth L. Wadlin, John A. Ramsen,
and Victor L. Vaughan, Jr.

Langley Aeronautical Laboratory
Langley Field, Va.

Washington
March 1954

NATIONAL ADVISORY COMMITTEE FOR AERONAUTICS

TECHNICAL NOTE 3079

THE HYDRODYNAMIC CHARACTERISTICS OF MODIFIED RECTANGULAR FLAT PLATES HAVING ASPECT RATIOS OF 1.00 AND 0.25 AND OPERATING NEAR A FREE WATER SURFACE

By Kenneth L. Wadlin, John A. Ramsen,
and Victor L. Vaughan, Jr.

SUMMARY

An investigation has been conducted to determine the hydrodynamic forces and moments acting on modified rectangular flat plates with aspect ratios of 1.00 and 0.25 mounted on a single strut and operating at several depths of submersion. A simple method has been developed by modification of Falkner's vortex-lattice theory which enables the prediction of the lift characteristics in unseparated flow at large depths. This method shows very good agreement with experimental data from the present tests and with aerodynamic data.

The experimental investigation indicated that decreasing the aspect ratio or depth of submersion caused a decrease in the lift coefficient, drag coefficient, and lift-drag ratio. The center of pressure moved forward with decreasing depth of submersion and aft with decreasing aspect ratio.

Two types of leading-edge separation at high angles were encountered. One type, called "white water" and found only for the aspect-ratio-1.00 surface, caused a slight decrease in the lift and moment coefficients and a slight increase in the drag coefficient. The other type, called the "planing bubble" and found for both surfaces, caused a sharp drop in the lift, drag, and moment characteristics of the order of that to be expected in the transition from the submerged to the planing condition.

INTRODUCTION

Interest has recently been shown in obtaining information on the force and moment characteristics of low-aspect-ratio lifting surfaces operating beneath the free water surface. In this connection, theoretical and experimental investigations have been undertaken by the National Advisory Committee for Aeronautics to determine methods of predicting the hydrodynamic characteristics of such surfaces and the effect

produced on these characteristics by the proximity of the free water surface.

The problem resolves itself into two parts: first, the determination of the characteristics at depths great enough so that effects of the free surface may be neglected, and second, the determination of the changes in the characteristics which occur as the free surface is approached.

The first part is essentially the same as the determination of the aerodynamic characteristics of a wing in an infinite incompressible medium. Therefore, with proper consideration of the Reynolds number, the large amount of aerodynamic theory and experimental data available for low-aspect-ratio lifting surfaces should be applicable in this case. Some of the aerodynamic theories and experimental data relating to low-aspect-ratio wings have been summarized in reference 1. In addition, the NACA has recently conducted investigations of a rectangular flat-plate wing of aspect ratio 0.25 (ref. 2) and of rectangular symmetrical wings of aspect ratios 1.0, 2.0, and 3.0 (ref. 3).

The second part of the problem, which is the determination of the effects of the proximity of the free water surface, represents the difference between the hydrodynamic and aerodynamic cases. In a confined space such as a towing tank, two additional effects must be considered, namely, the effect of the finite depth (which limits the speed of wave propagation) and the effect of the rigid side walls and bottom.

The purpose of this paper is to present the hydrodynamic characteristics of some low-aspect-ratio surfaces. Experimental data have been obtained in Langley tank no. 2 by using modified flat-plate surfaces with aspect ratios of 1.00 and 0.25 mounted on a single strut and operating at various depths of submersion. A simple modification introducing nonlinearity to existing aerodynamic theory has been developed in an attempt to provide a theory which will give reasonable agreement with the lift at great depths and also be amenable to possible modification with the method of images in order to include the effects of the free water surface. Comparisons between the experimental data at the large depths and this modified theory as well as comparisons with other existing aerodynamic theories are presented.

A description of several flow phenomena peculiar to this investigation is also presented together with the effects of these flow changes on the hydrodynamic characteristics. The comparison with the theory mentioned previously is not valid where the flow changes occurred and therefore is not made for these regions.

SYMBOLS

A	aspect ratio
$a_0, a_1, \ldots a_n$ $b_0, b_1, \ldots b_n$ $c_0, c_1, \ldots c_n$	unknown coefficients in vorticity-distribution series
b	span of lifting surface, ft
C_D	drag coefficient, $\frac{\text{Drag}}{\frac{1}{2}\rho V^2 S}$
C_L	lift coefficient, $\frac{\text{Lift}}{\frac{1}{2}\rho V^2 S}$
C_m	pitching-moment coefficient about trailing edge, $\frac{\text{Moment}}{\frac{1}{2}\rho V^2 Sc}$
c	chord of lifting surface, ft
F	position factor relating downwash control point to vortex, ft^{-1}
F_c	nondimensional position factor relating downwash control point to vortex, Fc
S	area of lifting surface, sq ft
V	forward velocity, ft/sec
w	downwash velocity, ft/sec
x, y	coordinates along the lifting surface, ft
x', y', z'	coordinates of downwash control point relative to vortex, ft
α	angle of attack, deg
Γ	circulation, ft^2/sec

γ vorticity, ft/sec

η dimensionless lateral coordinate, $2y/b$

θ dimensionless longitudinal coordinate, $\cos^{-1}\frac{2x}{c}$

ρ density, slugs/cu ft

The subscript 6 denotes a depth of submersion of 6 inches.

MODELS, APPARATUS, AND PROCEDURE

The models used were modified rectangular flat-plate surfaces with aspect ratios of 1.00 and 0.25 mounted on a single strut. In order to keep the effects of the finite thickness as small as possible, the leading edges of the plates were rounded to a 2:1 ellipse and the afterportions of the plates were symmetrically beveled so that the included angle at the trailing edge was 10°. A drawing of the models is shown in figure 1.

The strut, which can also be seen in figure 1, had an NACA 66_1-012 airfoil section. The strut was mounted perpendicular to the plates and intersected the upper surfaces without fillets. Both the plates and the strut were made of stainless steel and were polished to a smooth finish.

Tests were made by using the Langley tank no. 2 carriage and existing strain-gage balances which independently measured the lift, drag, and moment. The moment was measured about an arbitrary point above the model and the data thus obtained were used to calculate the moments about the trailing edge at the center line. The positive directions of forces, angles, and moments used in presenting the force data are shown in figure 2.

All tests were run with a wind screen which reduced aerodynamic tares and aerodynamic effects on flow patterns to negligible values. Before each run measurements were taken in the "at rest" condition with the model submerged and the values obtained were subtracted from all other data; thus, model buoyancy and strut buoyancy were not included in the data.

The force measurements were made at constant speeds for fixed angles of attack and depths of submersion. The depth of submersion is defined as the distance from the undisturbed water surface to the point on the model closest to the surface.

Tests were run at four depths of submersion (0.5 inch, 1.0 inch, 3.0 inches, and 6.0 inches) over a range of angles of attack from 0° to 20°. The range of speeds covered at each angle of attack and depth of submersion was limited by the capacities of the balances.

The change in angle of attack due to structural deflection caused by the lift and drag forces on the model was obtained during the calibration of the balances and the test data were adjusted accordingly. This change did not exceed 0.2° for most conditions although in a few cases changes up to 0.6° occurred. The depth of submersion was adjusted during each run to keep the change in this parameter to a minimum. The estimated accuracy of the measurements is as follows:

Angle of attack, deg	±0.1
Depth of submersion, in.	±0.05
Speed, ft/sec	±0.1
Lift, lb	±0.25
Drag, lb	±0.10
Moment, ft-lb	±0.5

The forces and moments were converted to the usual aerodynamic coefficient form by using a measured value of the density of 1.970 slugs/cu ft. The kinematic viscosity measured during the tests was 1.62×10^{-5} ft^2/sec.

EXPERIMENTAL RESULTS

General Force Data

The data obtained are presented in figures 3 to 8 as plots of lift, drag, and moment about the trailing edge as functions of the angle of attack with speed as a parameter. The data are presented for both aspect ratios at each of the four depths investigated.

The discontinuities in the drag curves at the low angles shown in figures 3 to 8 are due to changes in the flow which are invisible whereas the discontinuities in all the curves at the high angles are caused by flow changes which are visible. The visible flow changes and their effects on the characteristics are discussed later.

Results Outside the Range of Visible Flow Changes

Figure 9 shows the effect of aspect ratio on the lift and drag characteristics at a depth of 6.0 inches. At this depth, preliminary computations indicated that the effect of the free surface would be small.

The curves of lift coefficient against angle of attack show the nonlinearity common to low-aspect-ratio surfaces. This nonlinearity increased for a decrease in aspect ratio from 1.00 to 0.25. As would be expected, the lift coefficient decreased with the decrease in aspect ratio.

The curves of drag coefficient against lift coefficient indicate a slight decrease in drag coefficient for a given lift coefficient with increasing speed (Reynolds number) and a much greater decrease with the increase in aspect ratio. At a low value of lift coefficient for the aspect-ratio-0.25 surface, a change in the curve can be seen which corresponds to the discontinuity in the drag data for low angles of attack previously noted in figure 7. Because of the scale used, no such change is noticeable on this plot for the aspect-ratio-1.00 surface despite the fact that a discontinuity in the drag data occurred for this surface also (fig. 4). The change in the drag coefficient for the aspect-ratio-0.25 surface was sufficient to bring it below that for the aspect-ratio-1.00 surface at the low lift coefficients. Over most of the range of lift coefficients, however, the drag coefficient for the lower aspect ratio was the greater of the two. In this range the lift-drag ratios for given values of either lift coefficient or angle of attack were greater for the surface with the greater aspect ratio.

The effect of changing the depth of submersion on lift coefficient for both aspect ratios is shown in figure 10. Figure 10(a) presents values of the ratio of the lift coefficient at a given depth to the lift coefficient at a depth of 6 inches C_L/C_{L_6} plotted against angle of attack with depth of submersion as the parameter. The same ratio is plotted against depth of submersion with angle of attack as the parameter in figure 10(b). The lift coefficient decreased as the model approached the water surface, the decrease being greater for the higher aspect ratio. A change in the decrement with angle of attack may be noted, the minimum decrease occurring at about 12°. The decrement increased considerably as the angle of attack was reduced to 2° but only slightly as it was increased to 20°. A large part of the change at the lower angles of attack may be explained by recalling that the depth of submersion was measured near the leading edge. Thus, as the angle of attack was decreased for a given depth of submersion, the average depth of the plate decreased.

The effect of changing the depth of submersion on the drag coefficient is shown in figure 11 to be similar to the effect on the lift coefficient. Like the lift coefficient, the drag coefficient decreased as the model approached the water surface as would be expected because the induced drag coefficient, which is especially important at these low aspect ratios, is a function of the lift coefficient. The decrease again was greater for the higher aspect ratio and lower angles of attack, the minimum decrement occurring at about 12°.

Since the decrease in drag coefficient was less than the decrease in lift coefficient, the lift-drag ratio also decreased as the model approached the free water surface.

The curves of both lift- and drag-coefficient ratios against depth seem to approach the value at a depth of 6.0 inches asymptotically; this fact indicates that at the 6.0-inch depth the surface effect was negligible.

The location of the center of pressure as a function of the angle of attack with depth of submersion as a parameter is shown in figure 12 for both surfaces. In general, the center of pressure moved forward with decreasing angle of attack, decreasing depth of submersion, and increasing aspect ratio. The depth of submersion had a much greater effect at the lower angles of attack, the apparent center of pressure even occurring forward of the leading edge at the lowest angles of attack at 0.5- and 1.0-inch depths. These effects indicate an increase in negative pressure on the upper surface near the leading edge as the water surface is approached or the presence of a suction force over the aft portion of the bottom of the model at low angles of attack or both.

At the higher angles of attack for both models the center of pressure seems to be asymptotically approaching a point about 5/8 chord forward of the trailing edge. For the aspect-ratio-1.00 model, rearward movement of the center of pressure occurred at the low angles for depths of 3.0 and 6.0 inches.

Visible Flow Changes and Their Effects

Cavitation.- As was expected, cavitation at the leading edge occurred at high speeds for both aspect ratios for all depths. Sequence photographs of a typical run showing the formation of cavitation are presented in figure 13. At 30 feet per second no cavitation has occurred and the bright area at the leading edge in this instance is merely a reflection due to the lighting used. Although it cannot readily be seen in this figure, a slight widening of the bright area at 40 feet per second indicated the beginning of cavitation. The bright area is noticeably wider at 54 feet per second; at 62 feet per second, an area becomes evident at the ends of the leading edge where the cavitation is not so strong as in the middle portion of the cavitation region. This indicates that the low pressure in this area has been relieved somewhat. This area of pressure relief is still more in evidence at 70 feet per second. The area of pressure relief may have existed from the start of the cavitation but was so small as to be unnoticeable before 62 feet per second.

The angle of attack designated in this figure and all other sequence-photograph figures to follow is the angle of attack for the model at rest. Since the angle of attack changes with speed because of structural deflections, the photographs do not correspond exactly to a constant angle of attack.

The high speeds necessary for the inception of cavitation were reached only at very low angles of attack; therefore, the results of cavitation are not plainly evident in the data plots of figures 3 to 8.

Figure 14 shows a plot of lift coefficient C_L, drag coefficient C_D, and moment coefficient C_m against speed at the same conditions shown in figure 13. The lift coefficient and drag coefficient remain constant up to the speed of cavitation after which the lift coefficient gradually decreases with increasing speed while the drag coefficient increases. (The fact that the lift coefficient and drag coefficient coincide at speeds before the inception of cavitation is a coincidence peculiar only to the angle of attack illustrated.) The moment coefficient increases slightly up to cavitation speed but falls off at higher speeds.

Ventilation.- For both models at the higher angles of attack and the shallower depths, air was observed to enter the trailing vortices aft of the model. As the speed was increased the entrained air proceeded forward along a helical path inside the vortices until it reached the model when separation took place. The process is shown schematically in figure 15 in which the operation takes the form of a "planing bubble," an air bubble surrounded by a thin film of water in such a manner that no water touches the upper surface of the model.

For the aspect-ratio-1.00 model at a depth of 1 inch, the same process resulted in the formation of "white water," a foamy mixture of air and water which completely covered the upper surface of the model. This effect may be seen in the sequence photographs of figure 16. The helical airstream within the vortices is visible in the photograph taken at 10 feet per second whereas the white water is visible at 12.5 feet per second. When the speed was increased sufficiently, the white water changed to the planing bubble.

The effect of the formation of the white water on the force and moment characteristics is shown in figure 17. The lift coefficient increased until the formation of the white water, after which it decreased slightly and then leveled off. At angles of attack for which no white water formed, the lift coefficient increased up to approximately the speed at which the formation of the white water occurred at the higher angles of attack and then leveled off. Therefore, the principal change in lift coefficient introduced by the formation of the white water is the slight decrease after its formation. The drag coefficient remained more or less constant at the lower speeds, increased with the formation of the white water, and remained constant thereafter. At angles for which no white water occurred, no such drag rise was encountered. The moment coefficient increased at the lower speeds, decreased sharply with the formation of the white water, and then began to increase again. No sharp decrease was encountered at angles where no white water occurred.

For the aspect-ratio-1.00 model at 0.5-inch depth, the separation took either of the two forms: the white water described previously or the planing bubble which is shown in figure 18. The helical entrained airstream may be seen advancing within the vortices at 12 and 13 feet per second whereas at 15 feet per second the planing bubble has been formed. The model is, in effect, planing under the bubble since no water touches the upper surface. The corresponding force and moment characteristics are shown in figure 19. All three coefficients increase at the low speeds and then decrease sharply with the formation of the planing bubble, primarily because of the loss of all upper-surface lift. The decrease in lift coefficient is of the order of that to be expected for the transition from the submerged to the planing stage.

The ventilation boundaries for the aspect-ratio-1.00 surface at 0.5-inch depth are presented in figure 20 as a plot of angle of attack against speed. The present tests were run at constant angles of attack while increasing the speed; this procedure corresponds to moving from left to right along horizontal lines in this figure. Below 11.5° no separation was found. Along the line of planing-bubble inception designated A, the planing bubble was the only type of separation encountered. At angles above 12° the line of white-water inception was first encountered but as the speed was further increased the type of separation changed from the white water to the planing bubble as the line of secondary planing-bubble inception designated B was reached. The same type of planing bubble was obtained by crossing either line A or B. The difference in designation was adopted to indicate that in the case of line B the planing bubble was preceded by white water.

The tests indicated that, after the bubble was established, its persistence was very strong. Even in the case of the planing bubble following the white water, there was no tendency for the bubble to collapse or revert to the white water as the speed was decreased almost to standstill. If the speed were held constant and the angle of attack increased, which corresponds to proceeding upward along vertical lines in the figures, white water would occur only at speeds below about 13 feet per second when the white-water inception line was crossed. At speeds above 13 feet per second the planing bubble would occur as soon as the planing-bubble inception line A was crossed and would not change to white water with further increase in the angle of attack.

For the aspect-ratio-0.25 model, the white-water stage was not found for any combination of speed and angle tested. Instead, the separation always took the form of the planing bubble as shown in figure 21. The helical entrained airstream in the vortices can be seen at 10 feet per second, whereas at 15 feet per second the planing bubble has been formed. The boundary for the unventilated flow at a depth of submersion of 0.5 inch is shown in figure 22 and is similar to that

shown in figure 20 for the aspect-ratio-1.00 surface although displaced to higher speeds and higher angles.

From figure 23 it can be seen that, as the bubble forms, the lift, drag, and moment coefficients undergo a sharp decrease similar to the case for the aspect-ratio-1.00 model. However, all three coefficients decreased up to the speed where the planing bubble formed in contrast to the increase found for the aspect-ratio-1.00 model.

THEORY AND COMPARISON WITH EXPERIMENT

General

A theory was desired which would enable the determination of the lift at large depths and which would be amenable to possible modification by the method of images to account for the effects of the free water surface.

Bollay (ref. 4) and Weinig (ref. 5) have developed aerodynamic theories to apply to low-aspect-ratio surfaces. Flax and Lawrence (ref. 1), in addition to reviewing these and other low-aspect-ratio theories, have presented a semiempirical approach of their own. These theories, however, do not offer themselves readily to modification by the method of images so that an attempt was made to derive a more easily adaptable theory.

The method of Falkner (ref. 6), which is based on linear potential-flow theory, has been found to apply to a wide range of plan forms at high aspect ratio. The lifting surface in this method is replaced by a system of horseshoe vortices distributed both spanwise and chordwise and the method would lend itself to application of the method of images. Falkner's method was therefore modified to apply to low-aspect-ratio surfaces by introducing nonlinearity and some simplifications were introduced which apply to the present case. This modification is presented in the appendix of this paper.

Corrections to Experimental Data

In order to obtain an exact comparison between the data obtained in the present tests and the theories mentioned in the previous section, the tares and interferences would have to be eliminated. Their effect on the lift was expected to be small, however, so that comparisons with the data as obtained were deemed to be valid.

The finite water depth has an effect on the lift coefficient since it imposes a limitation on the speed of wave propagation. Previous experience indicates that the corrections necessary to account for this effect for the low aspect ratios under consideration may be assumed to be negligible. Computations were made to determine the effects of the solid boundaries by using an appropriate array of images. This method is a standard technique used in wind-tunnel work. (For example, see ref. 7.) Because of the small size of the models relative to the tank dimensions, these computations indicate that the effects of the solid boundaries may also be considered negligible.

Comparison With Experiment

The experimental results given in the present paper are compared with wind-tunnel test data and the theories mentioned in the preceding section in figures 24 and 25. Results of Falkner's linear theory (ref. 6) obtained by using two vortices spanwise and three vortices chordwise for the half-wing are also included.

Figure 24 shows the comparison for the aspect-ratio-0.25 surface. The experimental results given in reference 2 are generally lower than those of the present tests but agreement is still reasonable. The predictions of Falkner's linear theory are much lower than the experimental results at all angles but are nevertheless fair approximations for small angles. The theory of Bollay does not seem to have the general characteristics indicated by the data and predicts too high a lift coefficient for most of the range of angles covered. Weinig's method predicts values that are generally lower than the test points whereas the best agreement is provided by the theory of Flax and Lawrence and the method given in the present paper.

The comparison for the aspect-ratio-1.00 surface is presented in figure 25. The present data show excellent agreement with the experimental results of reference 3. The linear theory is again too low although agreement is better than for the lower aspect ratio. Bollay's theory, on the other hand, shows very poor correlation with the data. The theory of Flax and Lawrence gives good agreement at the lower angles but gives results which are considerably higher than the data at the higher angles. The theories of Weinig and the present paper show excellent agreement with the data, the theory of the present paper being slightly superior at the higher angles.

On an overall basis, then, the comparison indicates that the Bollay theory is not very accurate for either aspect ratio 1.00 or 0.25 although it begins to approach reasonable accuracy as the aspect ratio is reduced. On the other hand, the linear theory is also inaccurate for both aspect ratios but becomes better as the aspect ratio is increased. The theories

of Flax and Lawrence, Weinig, and the present paper show reasonable agreement for both aspect ratios, the present theory being slightly more accurate on an overall basis. The Flax and Lawrence theory gives only fair agreement at the higher angles for the aspect-ratio-1.00 surface whereas the Weinig theory gives only fair agreement at the higher angles for the aspect-ratio-0.25 surface. The present theory appears to offer possibilities of modification to include the effects of proximity of the free water surface by the method of images. Both the Weinig and the Flax and Lawrence theories would be difficult to modify in this manner.

CONCLUSIONS

A simple method has been developed by modification of Falkner's vortex-lattice theory to predict the lift characteristics for unseparated flow at large depths. This method shows good agreement with data from tank tests and wind-tunnel tests for aspect ratios of 1.00 and 0.25.

An experimental investigation of the hydrodynamic forces and moments acting on aspect-ratio-1.00 and aspect-ratio-0.25 modified rectangular flat plates mounted on a single strut and operating at several depths of submersion indicated that:

Decreasing the aspect ratio for a given angle of attack and depth of submersion decreased the lift coefficient, the drag coefficient, and the lift-drag ratio and caused a rearward movement of the center of pressure.

Decreasing the depth of submersion for a given aspect ratio and angle of attack decreased the lift coefficient, drag coefficient, and lift-drag ratio and caused a forward movement of the center of pressure.

A high-angle type of separation at the leading edge called "white water" and found only for the aspect-ratio-1.00 surface caused a slight decrease in lift coefficient and moment coefficient and a slight increase in the drag coefficient.

Another high-angle type of separation at the leading edge called the "planing bubble" and found for both aspect ratios caused a sharp

decrease in lift, drag, and moment coefficients of the order of that to be expected in the transition from the submerged to the planing conditions.

Langley Aeronautical Laboratory,
National Advisory Committee for Aeronautics,
Langley Field, Va., January 19, 1954.

APPENDIX

MODIFICATION OF FALKNER'S THEORY

The vorticity distribution in the Falkner method is expressed by the double series

$$\gamma = \frac{4bV \tan \alpha}{c}\sqrt{1 - \eta^2}\left[\cot \frac{\theta}{2}\left(a_0 + a_1\eta + a_2\eta^2 + \ldots\right) + \sin \theta\left(b_0 + b_1\eta + b_2\eta^2 + \ldots\right) + \sin 2\theta\left(c_0 + c_1\eta + c_2\eta^2 + \ldots\right) + \ldots\right] \quad (1)$$

where the variables are defined in the following sketch:

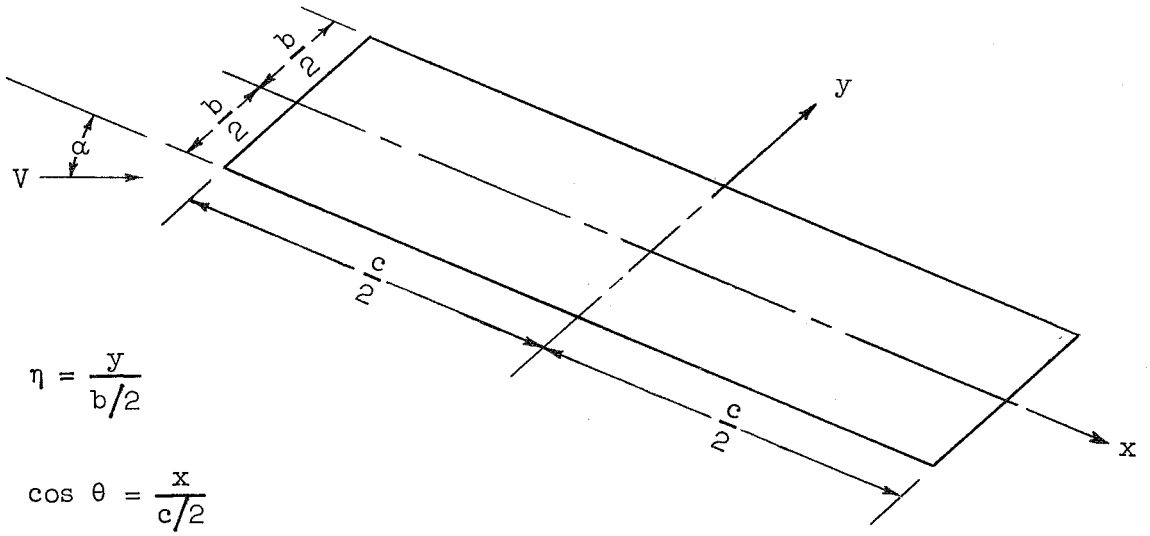

$$\eta = \frac{y}{b/2}$$

$$\cos \theta = \frac{x}{c/2}$$

For the symmetrical case such as the present one, the odd powers of η vanish. The circulation is expressed by

$$\Gamma = \int_{-c/2}^{c/2} \gamma \, dx$$

which now becomes

$$\Gamma = \frac{4bV \tan \alpha}{c}\sqrt{1 - \eta^2}\left[\left(a_0 + a_2\eta^2 + \ldots\right)\int_{-c/2}^{c/2} \cot \frac{\theta}{2}\, dx + \right.$$

$$\left(b_0 + b_2\eta^2 + \ldots\right)\int_{-c/2}^{c/2} \sin \theta\, dx +$$

$$\left.\left(c_0 + c_2\eta^2 + \ldots\right)\int_{-c/2}^{c/2} \sin 2\theta\, dx + \ldots\right] \qquad (2)$$

But

$$\frac{x}{c} = \frac{\cos \theta}{2}$$

so that

$$d\left(\frac{x}{c}\right) = -\frac{1}{2} \sin \theta\, d\theta$$

and

$$\cot \frac{\theta}{2} = \frac{1 + \cos \theta}{\sin \theta}$$

Therefore,

$$\int_{-c/2}^{c/2} \cot \frac{\theta}{2}\, dx = c\int_{-1/2}^{1/2} \cot \frac{\theta}{2}\, d\left(\frac{x}{c}\right)$$

$$= -\frac{c}{2}\int_{\pi}^{0} (1 + \cos \theta)d\theta$$

$$= \frac{\pi c}{2}$$

Similarly,

$$\int_{-c/2}^{c/2} \sin \theta \, dx = \frac{\pi c}{4}$$

and

$$\int_{-c/2}^{c/2} \sin n\theta \, dx = 0$$

where $n > 1$. Therefore,

$$\Gamma = 4bV\sqrt{1 - \eta^2}\tan \alpha\left[\frac{\pi}{2}\left(a_0 + a_2\eta^2 + \ldots\right) + \frac{\pi}{4}\left(b_0 + b_2\eta^2 + \ldots\right)\right] \qquad (3)$$

Now,

$$\text{Lift} = \int_{-b/2}^{b/2} \rho V\Gamma \, dy$$

and

$$C_L = \int_{-b/2}^{b/2} \frac{\rho V\Gamma}{\frac{\rho}{2} V^2 S} \, dy = \frac{b}{VS} \int_{-1}^{1} \Gamma \, d\eta$$

Hence,

$$C_L = \frac{b}{VS} \int_{-1}^{1} 4bV\sqrt{1 - \eta^2}\tan \alpha\left[\frac{\pi}{2}\left(a_0 + a_2\eta^2 + \ldots\right) + \frac{\pi}{4}\left(b_0 + b_2\eta^2 + \ldots\right)\right] d\eta$$

$$C_L = \frac{2b^2\pi}{S} \tan \alpha \int_{-1}^{1} \sqrt{1 - \eta^2}\left[\left(a_0 + \frac{b_0}{2}\right) + \left(a_2 + \frac{b_2}{2}\right)\eta^2 + \ldots\right] d\eta$$

$$C_L = \frac{b^2\pi^2}{S} \tan \alpha \left[\left(a_0 + \frac{b_0}{2} \right) + \frac{1}{4} \left(a_2 + \frac{b_2}{2} \right) + \frac{1}{8} \left(a_4 + \frac{b_4}{2} \right) + \ldots \right] \quad (4)$$

The evaluation of the unknowns a_n, b_n, and so forth is accomplished as follows:

(1) The vorticity is concentrated into an appropriate number of horseshoe vortices distributed chordwise and spanwise and expressed in terms of equation (1).

(2) At a number of control points, the downwash due to all the vortices as found from the Biot-Savart law is summed.

(3) The downwash angle thus determined at each control point is equated to the local slope of the wing at that control point.

(4) The resulting equations are solved simultaneously for a_n, b_n, and so forth.

The results obtained by the methods used thus far are applicable to any wing shape or aspect ratio by choosing the proper vortex-lattice distribution. Because of the particular models being considered in the present paper, several simplifying assumptions were introduced.

Because of the low aspect ratios under investigation, the assumption is made that the vortices are concentrated so that spanwise only one vortex occurs whose center is at the plane of symmetry. The use of a single vortex means that the terms representing the spanwise distribution may be reduced to one at each chordwise location. This assumption reduces equation (1) to

$$\gamma = \frac{4bV \tan \alpha}{c} \sqrt{1 - \eta^2} \left[a_0 \cot \frac{\theta}{2} + b_0 \sin \theta + c_0 \sin 2\theta + \ldots \right] \quad (5)$$

The $\cot \frac{\theta}{2}$ term applies for the straight-line airfoil and the $\sin n\theta$ terms are in effect corrective terms for deviations from the straight line. In order to simplify the equation further, the surfaces are assumed to be represented by the $\cot \frac{\theta}{2}$ term only; this assumption means that the surfaces are now represented by one horseshoe vortex. The final equation for the vorticity therefore is

$$\gamma = \frac{4bV \tan \alpha}{c} \sqrt{1 - \eta^2}\, a_0 \cot \frac{\theta}{2} \quad (6)$$

In a manner similar to that used in obtaining equation (3), the circulation is obtained as

$$\Gamma = \frac{4bV \tan \alpha}{c} \sqrt{1 - \eta^2}\, a_0 \frac{\pi c}{2}$$

or

$$\Gamma = 2\pi bVa_0 \sqrt{1 - \eta^2} \tan \alpha \tag{7}$$

According to Glauert (ref. 8), the downwash produced by a simple horseshoe vortex may be expressed by

$$w = \frac{\Gamma}{4\pi} F \tag{8}$$

where F is a position factor which is governed by the relative location of the horseshoe vortex and the point at which the downwash is computed. Combining equations (7) and (8) and setting $\eta = 0$, since the vortex is centered at the plane of symmetry, gives

$$\frac{w}{V} = \frac{a_0 bF \tan \alpha}{2} \tag{9}$$

Equating this relation to the local slope of the plate, which is $\tan \alpha$, yields

$$a_0 = \frac{2}{bF}$$

or in nondimensional form

$$a_0 = \frac{2}{F_c A} \tag{10}$$

where

$$F_c = Fc$$

and

$$A = \frac{b}{c}$$

By applying the methods used in obtaining equation (4), the following equation results:

$$C_L = \frac{b}{VS}\int_{-1}^{1} \Gamma \, d\eta$$

Substituting equation (7) into this equation yields

$$C_L = \frac{2\pi b^2}{S} a_0 \tan \alpha \int_{-1}^{1} \sqrt{1 - \eta^2} d\eta$$

or

$$C_L = \frac{2\pi^2 b^2}{2S} a_0 \tan \alpha \tag{11}$$

Substituting equation (10) into equation (11) and using the relation $S = bc$ yields

$$C_L = \frac{2\pi^2 \tan \alpha}{F_c} \tag{12}$$

Thus, the only unknown necessary to determine the lift coefficient as a function of the angle of attack is the position factor F_c.

From reference 8, F is given as

$$F = \frac{x'}{(x')^2 + (z')^2}\left[\frac{y' + \frac{b}{2}}{\sqrt{(x')^2 + (z')^2 + \left(y' + \frac{b}{2}\right)^2}} - \frac{y' - \frac{b}{2}}{\sqrt{(x')^2 + (z')^2 + \left(y' - \frac{b}{2}\right)^2}}\right] -$$

$$\frac{y' - \frac{b}{2}}{(z')^2 + \left(y' - \frac{b}{2}\right)^2}\left[1 + \frac{x'}{\sqrt{(x')^2 + (z')^2 + \left(y' - \frac{b}{2}\right)^2}}\right] +$$

$$\frac{y' + \frac{b}{2}}{(z')^2 + \left(y' + \frac{b}{2}\right)^2}\left[1 + \frac{x'}{\sqrt{(x')^2 + (z')^2 + \left(y' + \frac{b}{2}\right)^2}}\right] \tag{13}$$

where the variables are defined by the following sketch:

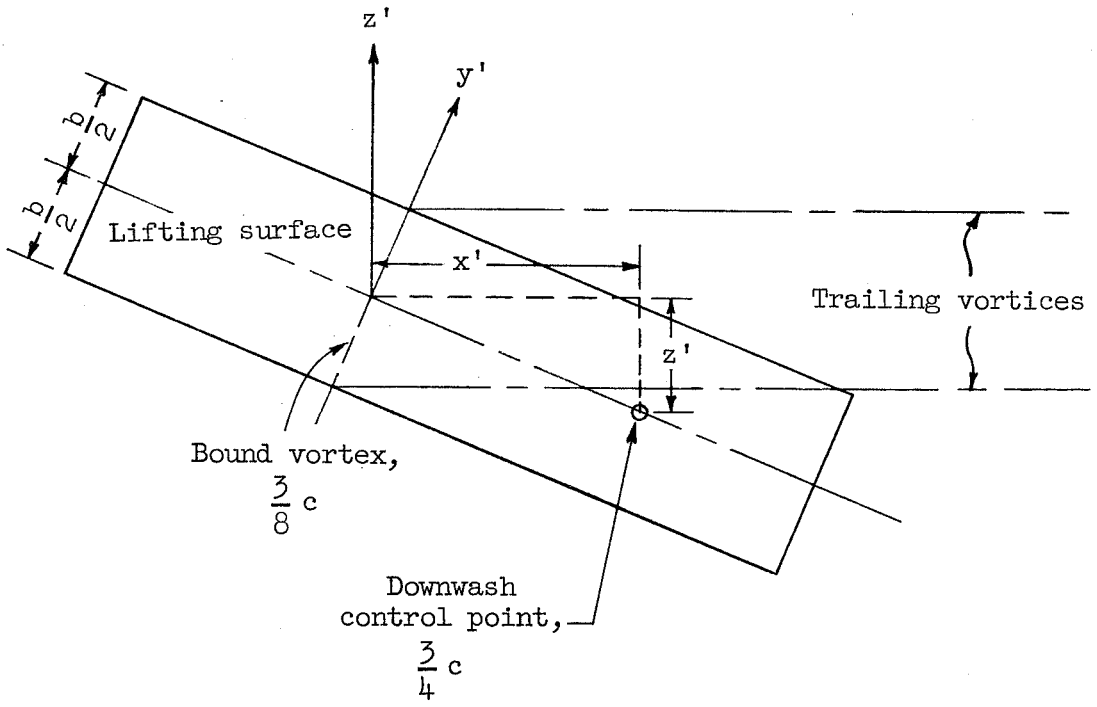

From the assumptions made previously, $y' = 0$. The single horseshoe vortex is considered to operate at the 3/8-chord point (which is the center of pressure at high angles for both surfaces tested) and the downwash is summed at the 3/4-chord point. The nonlinearity is now introduced by considering the displacements produced by changing the angle of attack.

Substituting

$$x' = \frac{3c}{8} \cos \alpha$$

$$y' = 0$$

$$z' = \frac{3c}{8} \sin \alpha$$

into equation (13) yields

$$F = \frac{\cos \alpha}{\frac{3c}{8}}\left[\frac{b}{\sqrt{\left(\frac{3c}{8}\right)^2 + \frac{b^2}{4}}}\right] + \frac{b}{\left(\frac{3c}{8}\right)^2 \sin^2\alpha + \frac{b^2}{4}}\left[1 + \frac{\frac{3c}{8}\cos \alpha}{\sqrt{\left(\frac{3c}{8}\right)^2 + \frac{b^2}{4}}}\right] \qquad (14)$$

Expressing all measurements in chords and using the fact that $A = \frac{b}{c}$ gives

$$F_c = \frac{8A \cos \alpha}{3\sqrt{\left(\frac{3}{8}\right)^2 + \frac{A^2}{4}}} + \frac{A}{\left(\frac{3}{8}\sin \alpha\right)^2 + \frac{A^2}{4}}\left[1 + \frac{\frac{3}{8}\cos \alpha}{\sqrt{\left(\frac{3}{8}\right)^2 + \frac{A^2}{4}}}\right]$$

Clearing of fractions gives

$$F_c = \frac{64A \cos \alpha}{3\sqrt{9 + 16A^2}} + \frac{64A}{9 \sin^2\alpha + 16A^2}\left(1 + \frac{3 \cos \alpha}{\sqrt{9 + 16A^2}}\right) \qquad (15)$$

Solving equation (15) and entering the value of F_c for any particular case into equation (12) now enables the determination of the lift coefficient. These expressions are used in making the computations, the results of which are shown in figures 24 and 25.

REFERENCES

1. Flax, A. H., and Lawrence, H. R.: The Aerodynamics of Low-Aspect-Ratio Wings and Wing-Body Combinations. Rep. No. CAL-37, Cornell Aero. Lab., Inc., Sept. 1951.

2. Michael, William H., Jr.: Flow Studies in the Vicinity of a Modified Flat-Plate Rectangular Wing of Aspect Ratio 0.25. NACA TN 2790, 1952.

3. Jones, George W., Jr.: Investigation of the Effects of Variations in the Reynolds Number Between 0.4×10^6 and 3.0×10^6 on the Low-Speed Aerodynamic Characteristics of Three Low-Aspect-Ratio Symmetrical Wings With Rectangular Plan Forms. NACA RM L52G18, 1952.

4. Bollay, William: A Non-Linear Wing Theory and Its Application to Rectangular Wings of Small Aspect Ratio. Z.f.a.M.M., Bd. 19, Nr. 1, Feb. 1939, pp. 21-35.

5. Weinig, F.: Lift and Drag of Wings With Small Span. NACA TM 1151, 1947.

6. Falkner, V. M.: The Calculation of Aerodynamic Loading on Surfaces of Any Shape. R. & M. No. 1910, British A.R.C., 1943.

7. Theodorsen, Theodore: The Theory of Wind-Tunnel Wall Interference. NACA Rep. 410, 1931.

8. Glauert, H.: The Elements of Aerofoil and Airscrew Theory. Cambridge Univ. Press, 1926, p. 158.

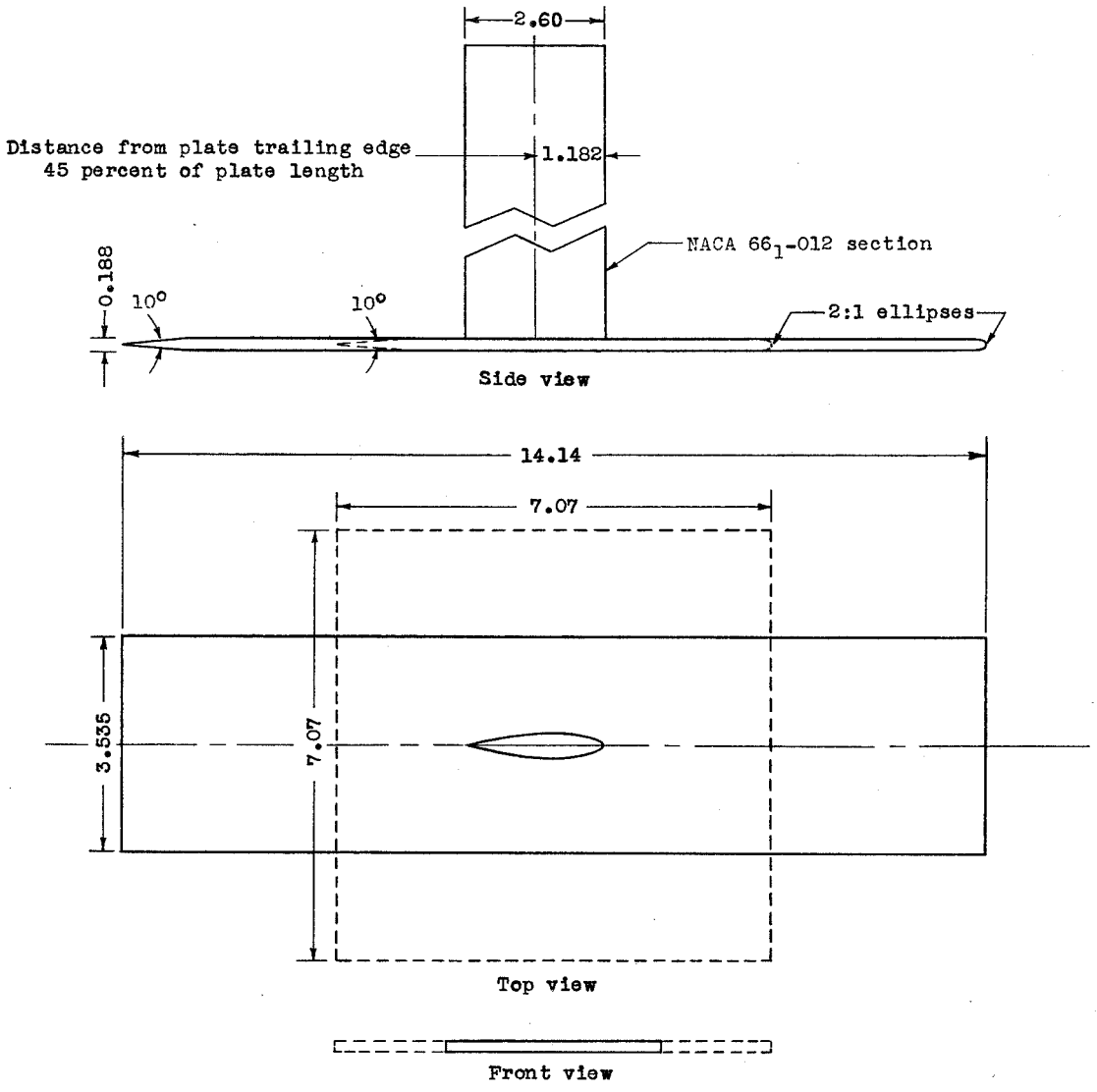

Figure 1.- Details of the models. (Dimensions are in inches.)

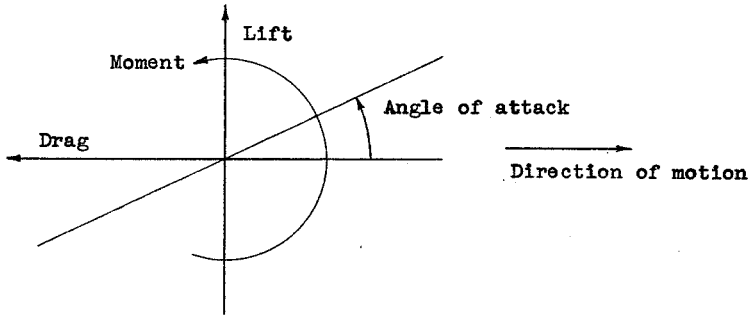

Figure 2.- System of axes. (Arrows indicate positive directions of forces, moments, and angles.)

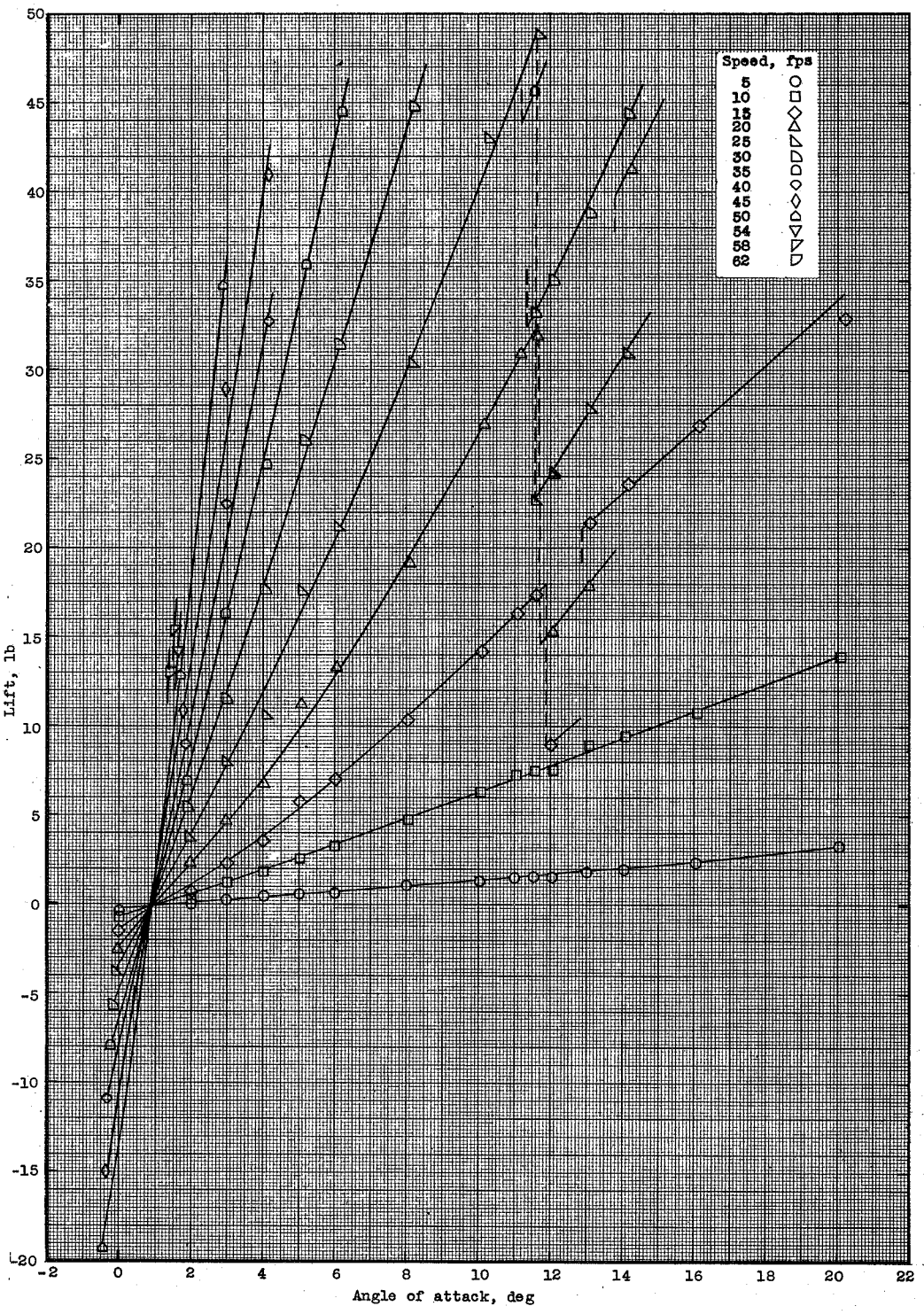

(a) Depth of submersion, 0.5 inch.

Figure 3.- Lift on the aspect-ratio-1.00 flat plate mounted on a single strut.

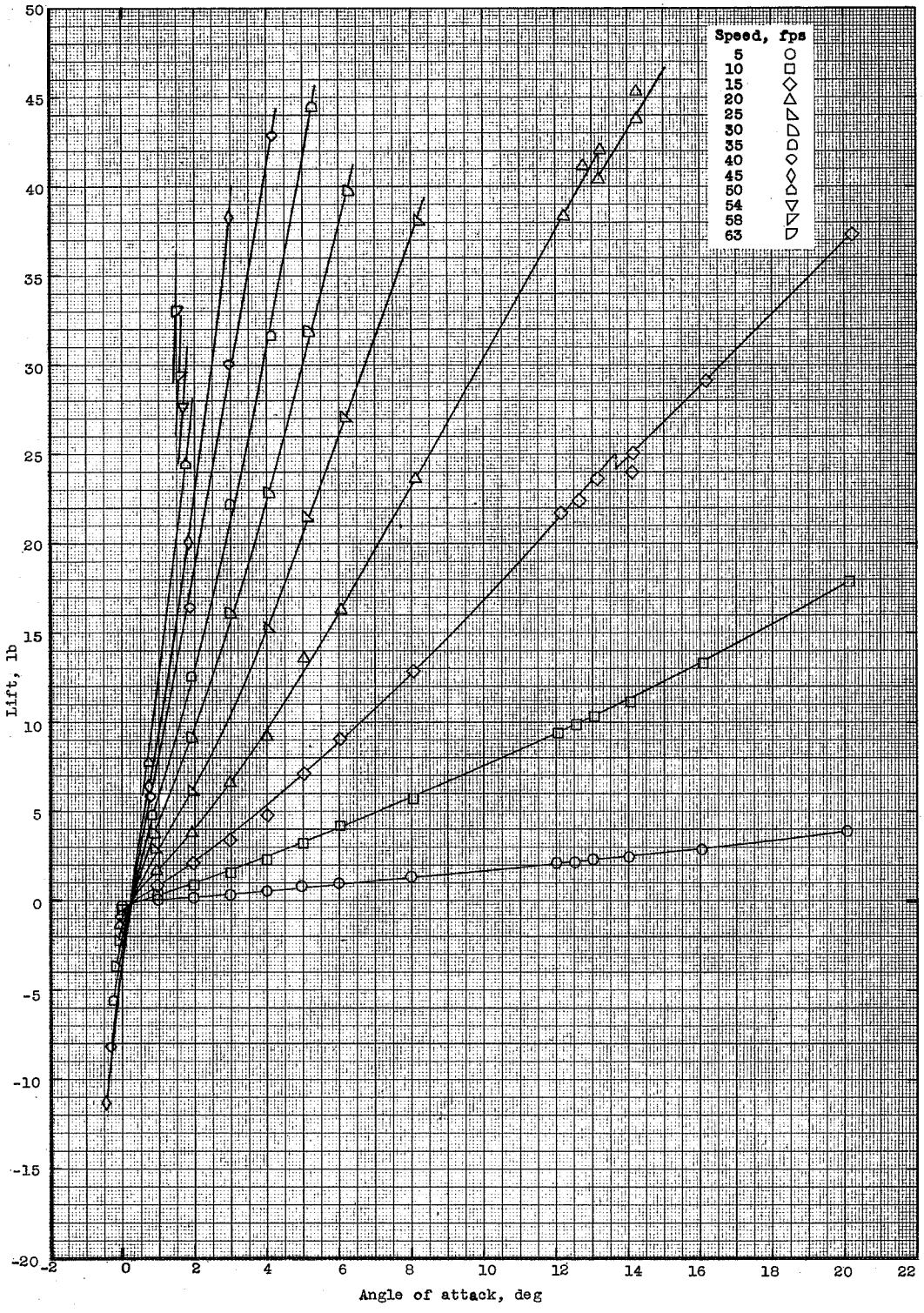

(b) Depth of submersion, 1.0 inch.

Figure 3.- Continued.

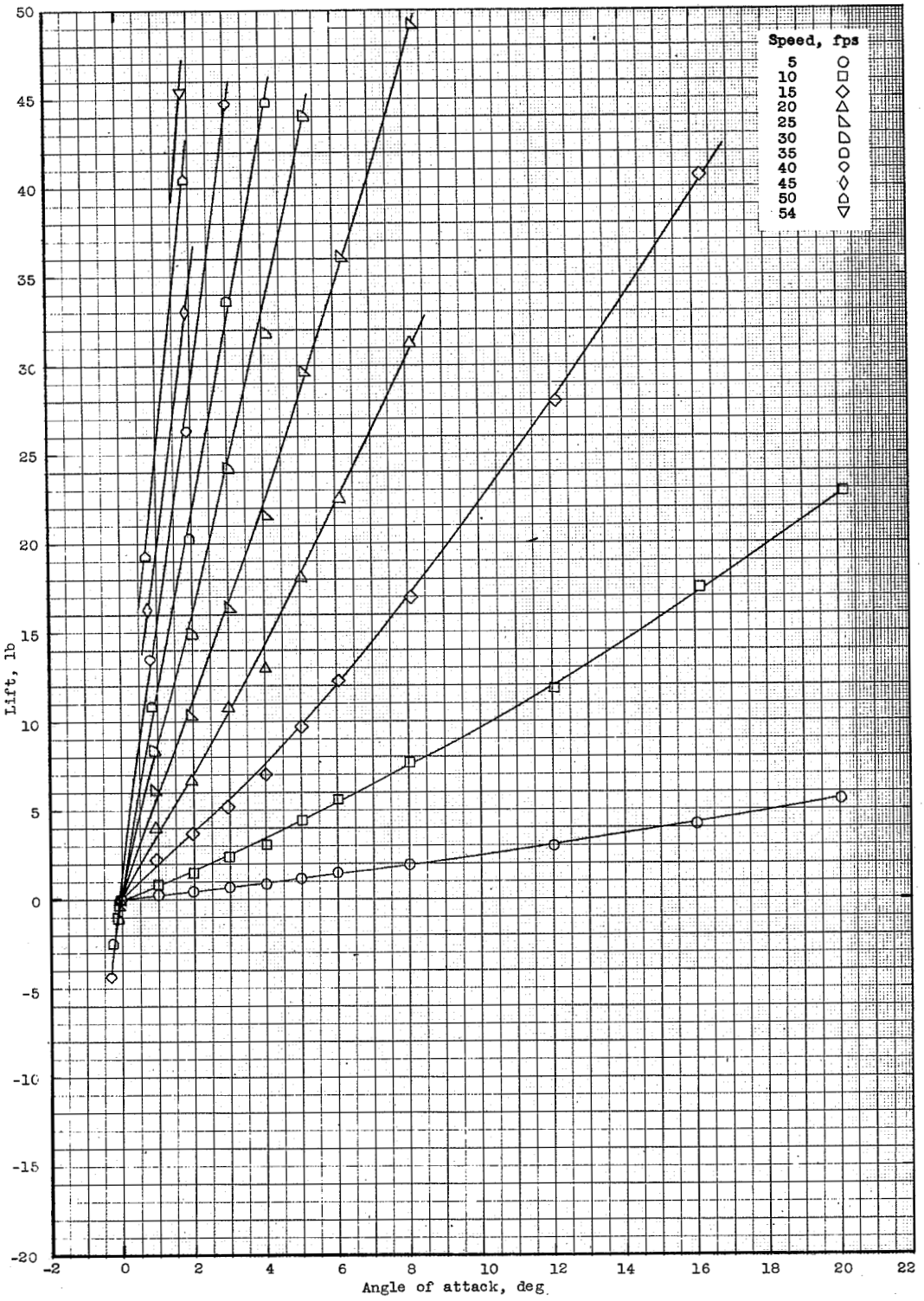

(c) Depth of submersion, 3.0 inches.

Figure 3.- Continued.

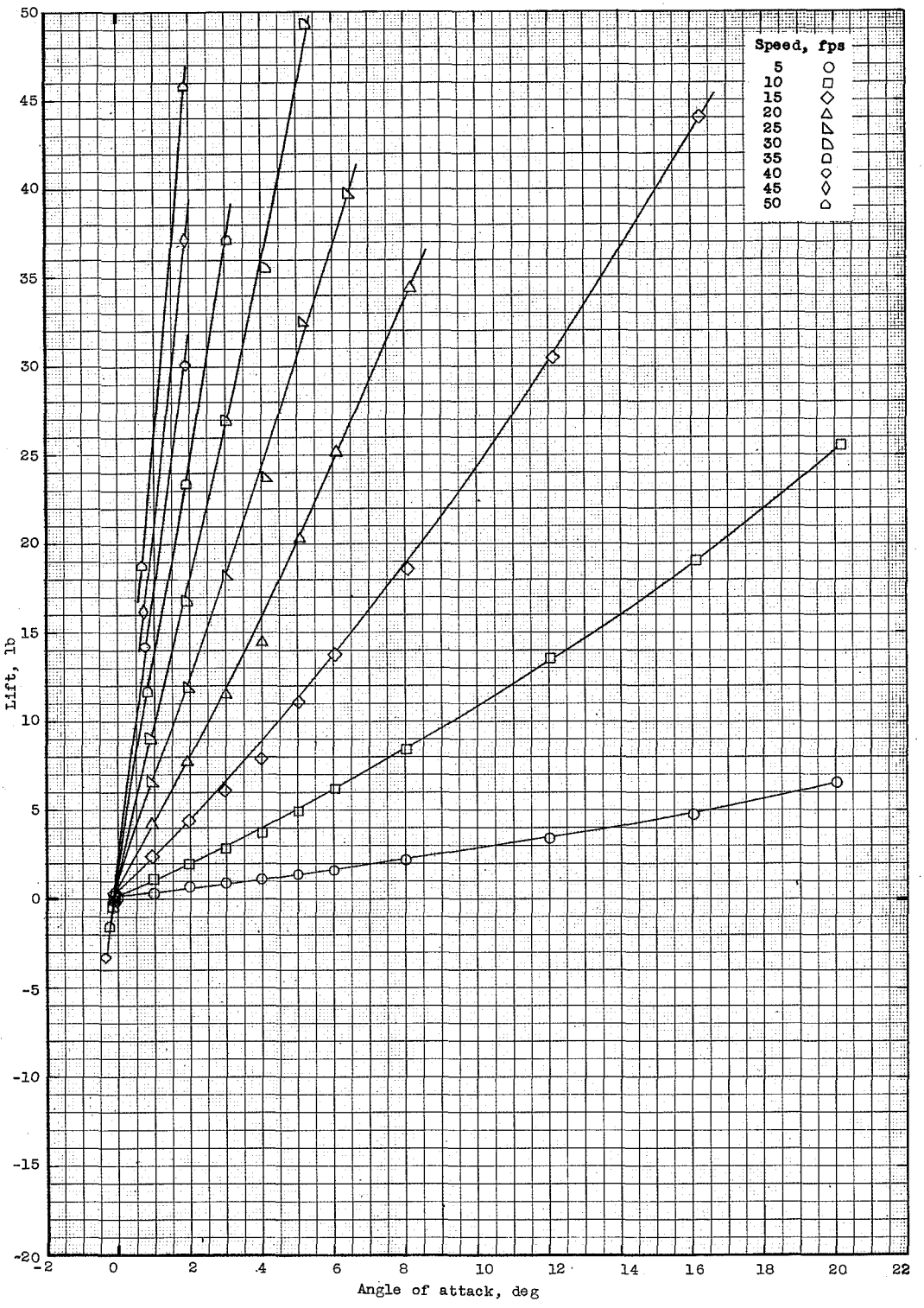

(d) Depth of submersion, 6.0 inches.

Figure 3.- Concluded.

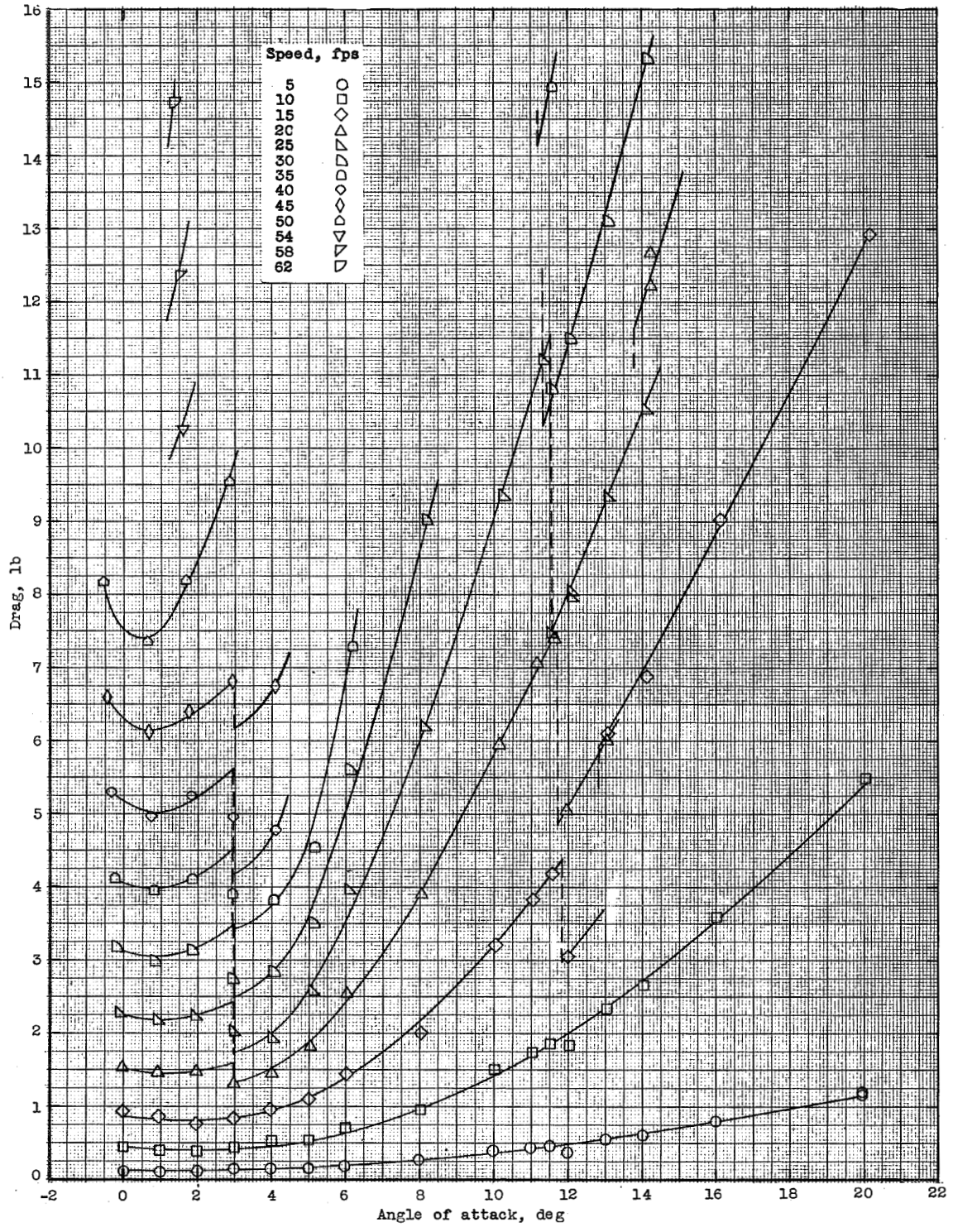

(a) Depth of submersion, 0.5 inch.

Figure 4.- Drag on the aspect-ratio-1.00 flat plate mounted on a single strut.

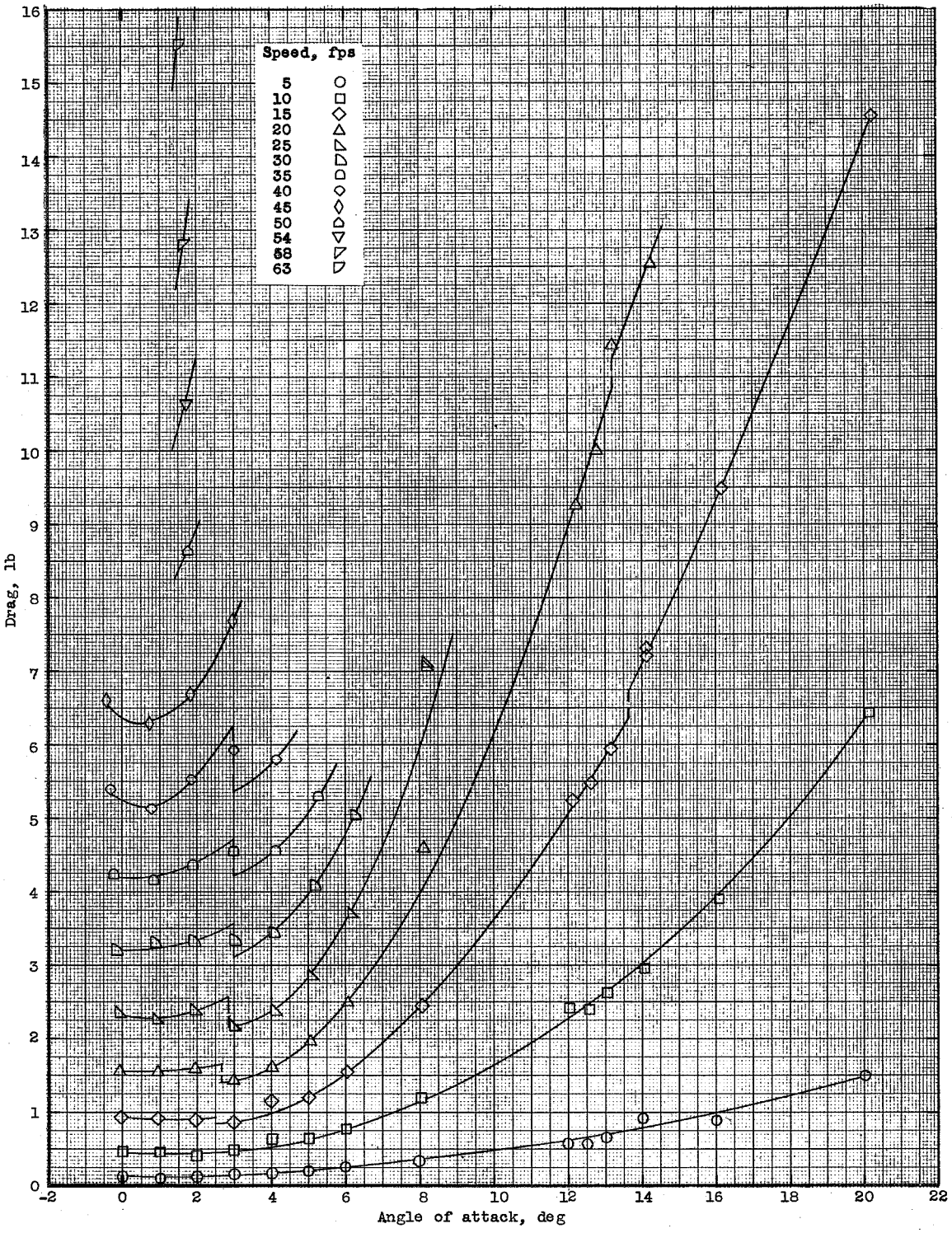

(b) Depth of submersion, 1.0 inch.

Figure 4.- Continued.

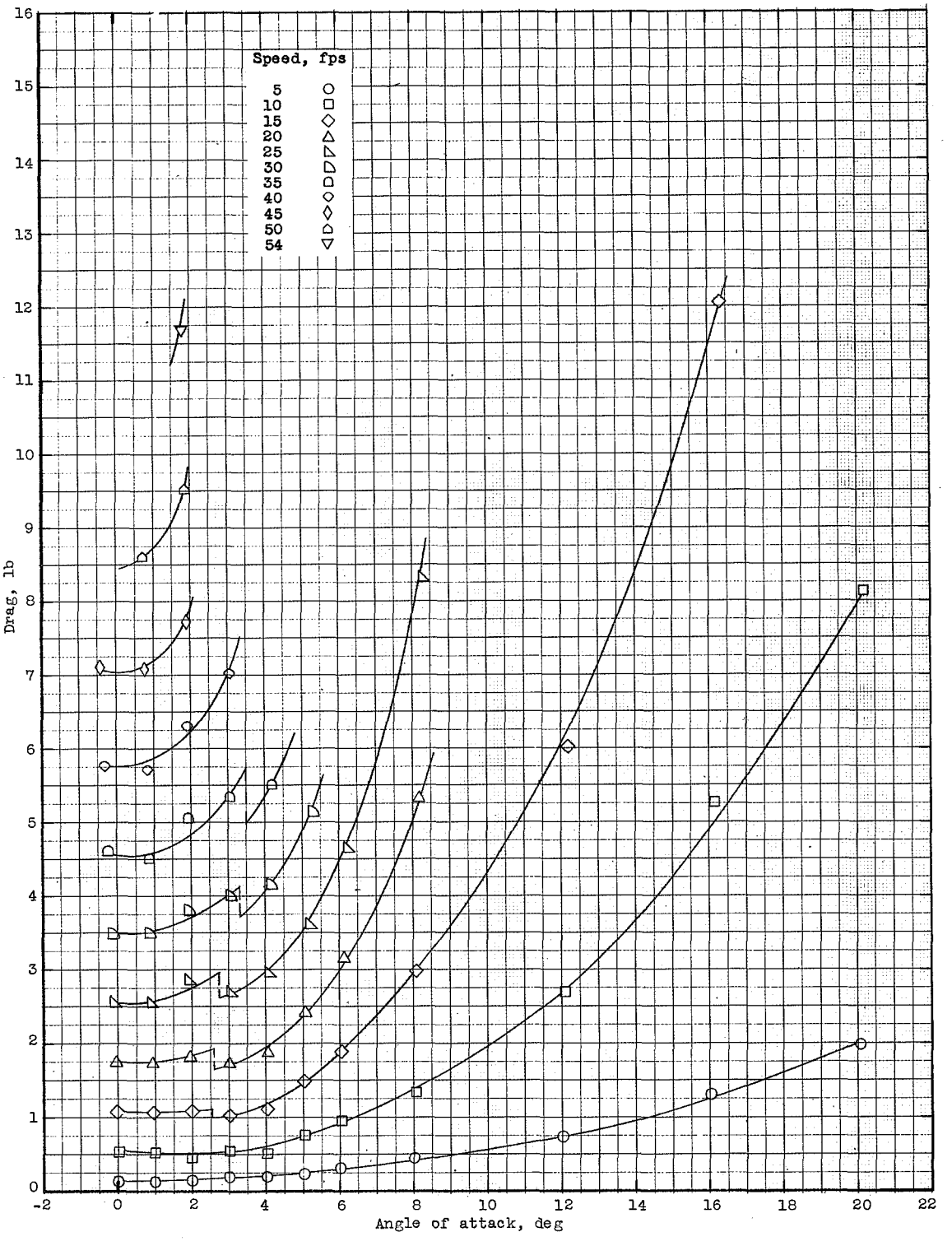

(c) Depth of submersion, 3.0 inches.

Figure 4.- Continued.

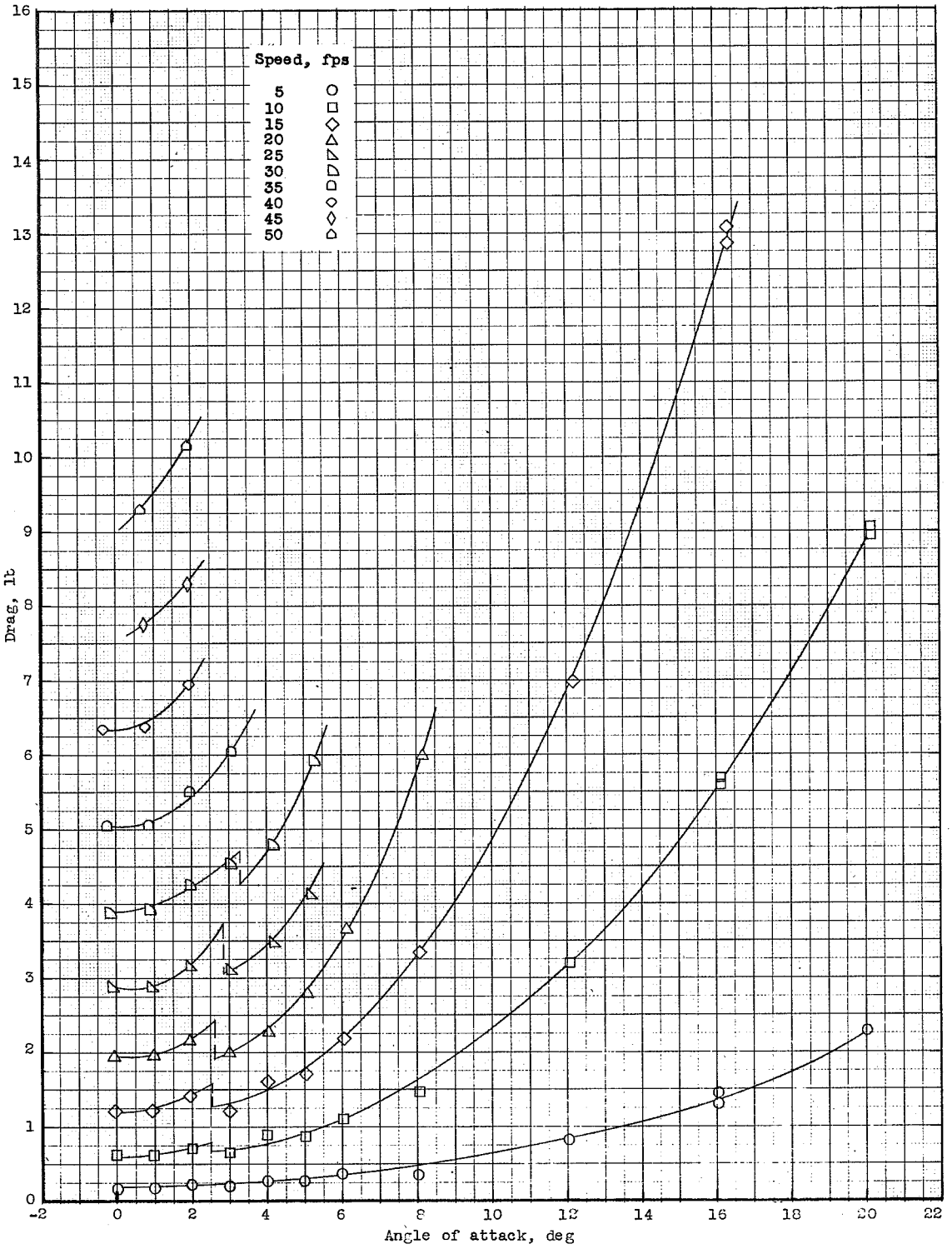

(d) Depth of submersion, 6.0 inches.

Figure 4.- Concluded.

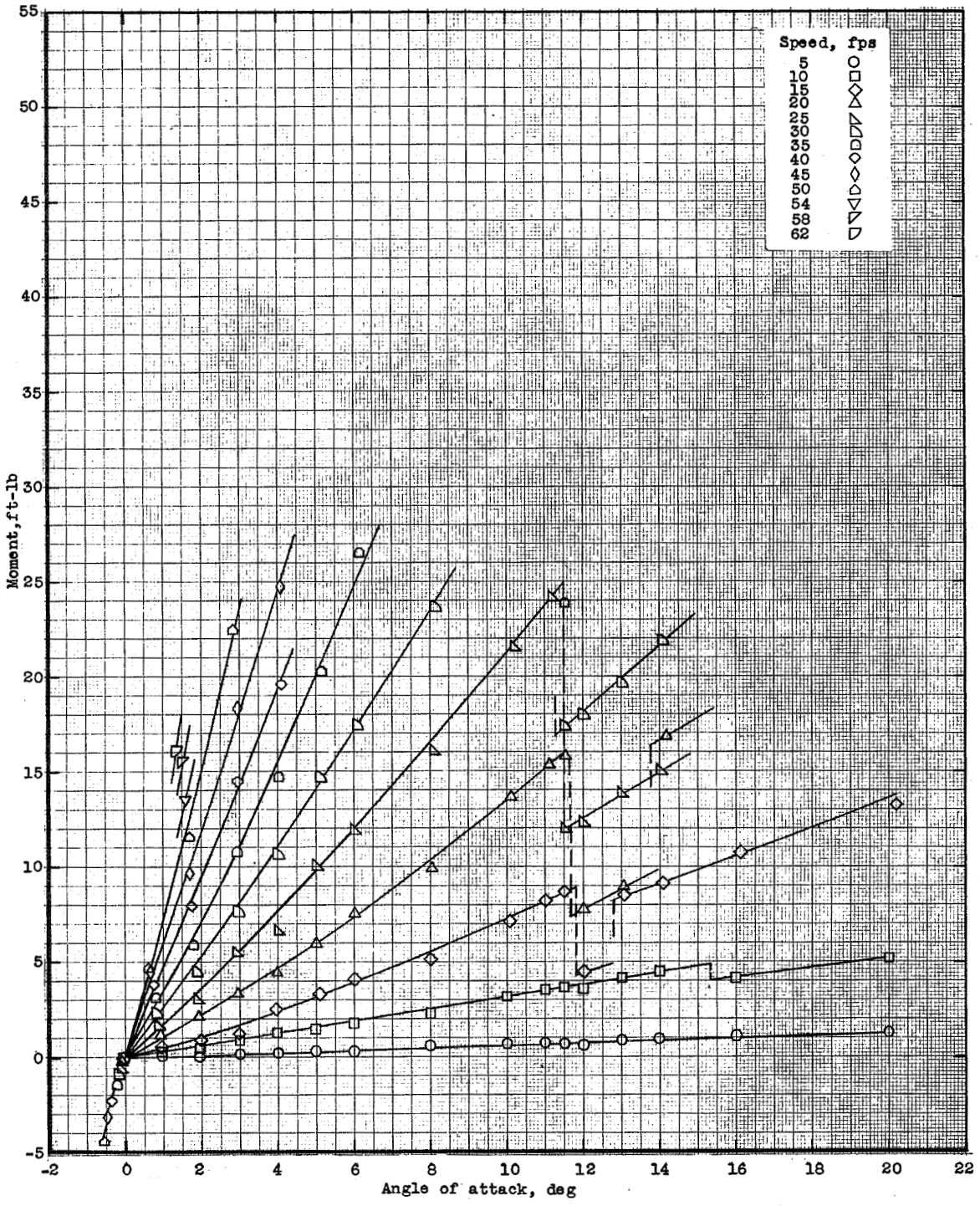

(a) Depth of submersion, 0.5 inch.

Figure 5.- Moment on the aspect-ratio-1.00 flat plate mounted on a single strut.

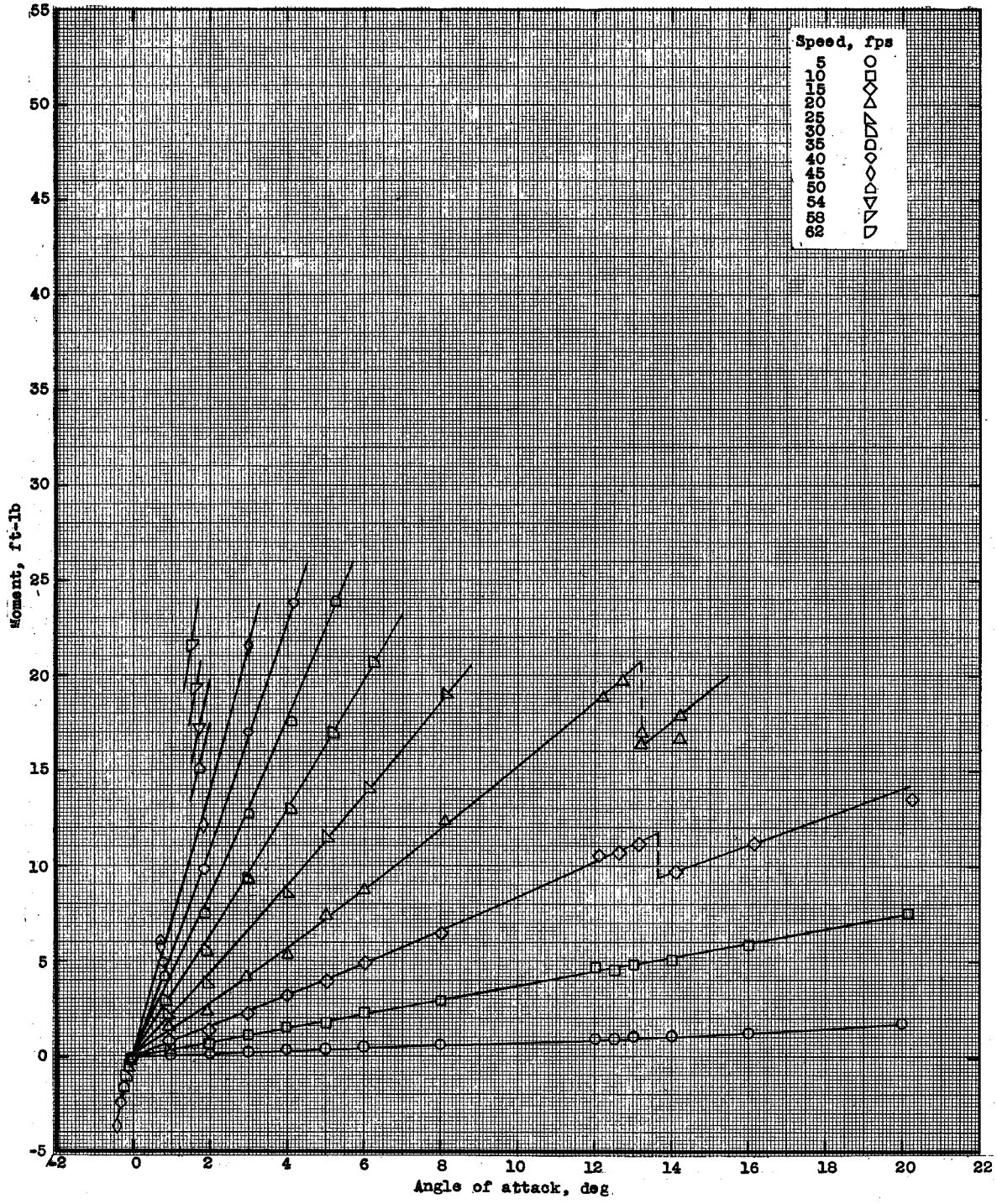

(b) Depth of submersion, 1.0 inch.

Figure 5.- Continued.

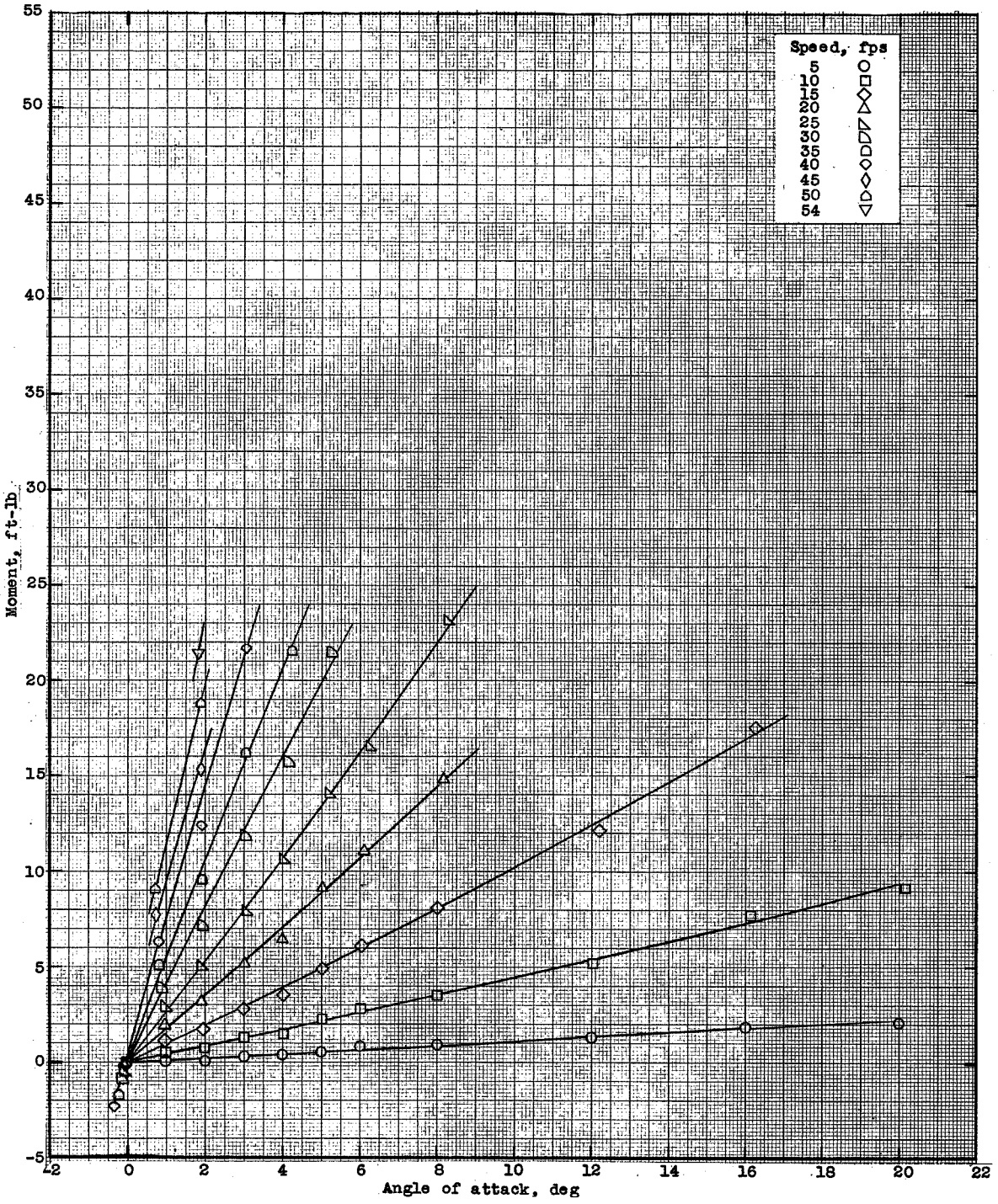

(c) Depth of submersion, 3.0 inches.

Figure 5.- Continued.

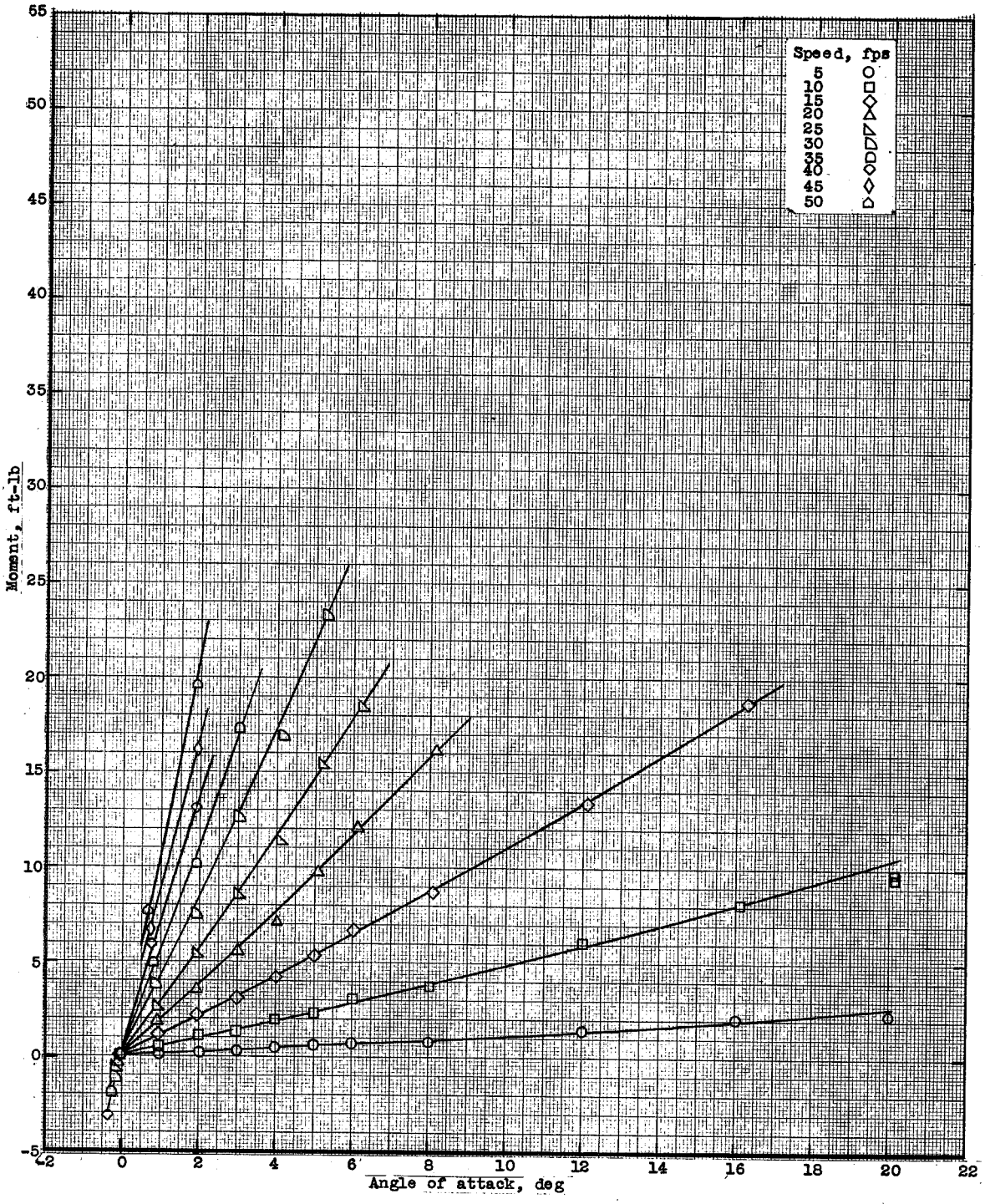

(d) Depth of submersion, 6.0 inches.

Figure 5.- Concluded.

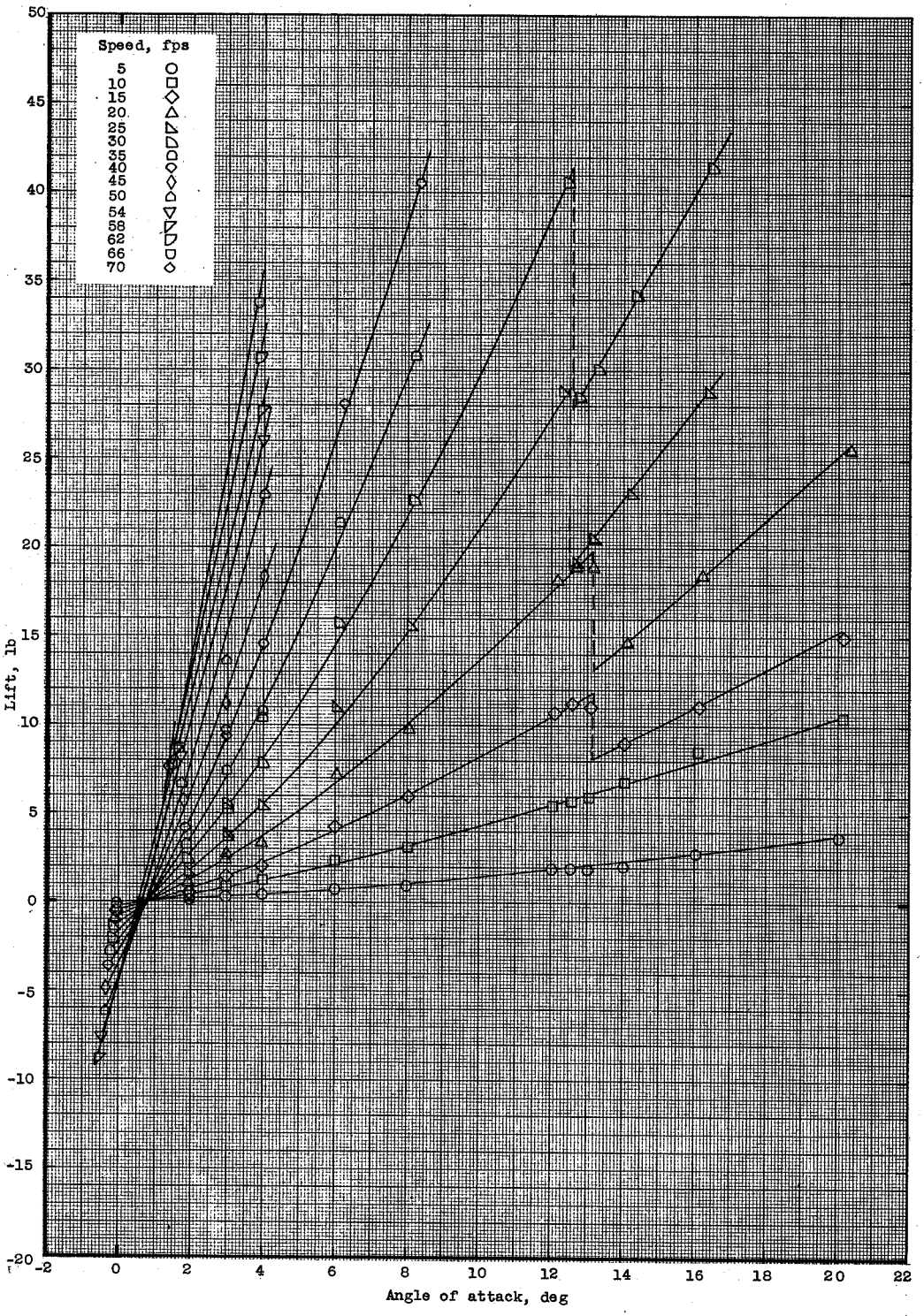

(a) Depth of submersion, 0.5 inch.

Figure 6.- Lift on the aspect-ratio-0.25 flat plate mounted on a single strut.

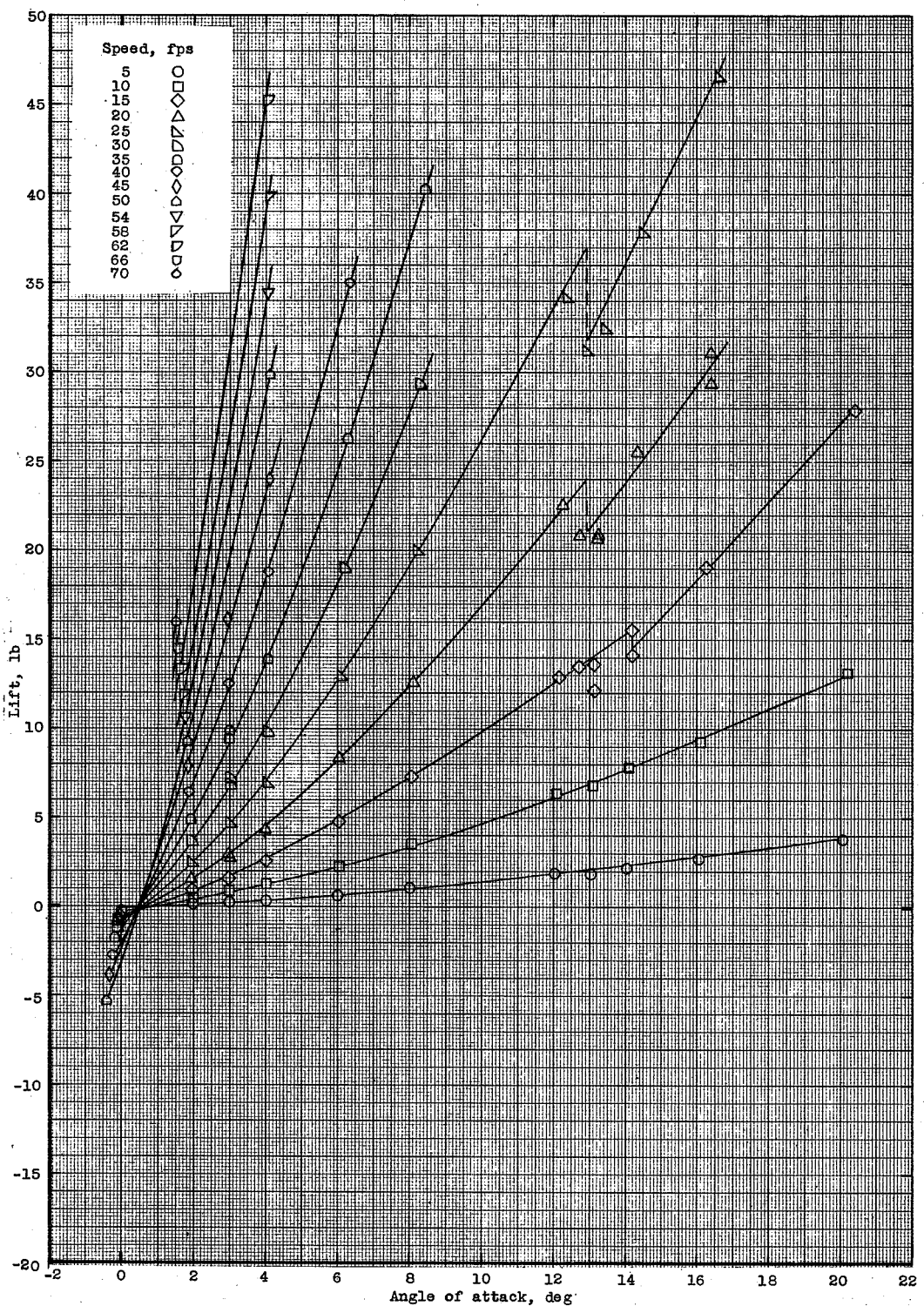

(b) Depth of submersion, 1.0 inch.

Figure 6.- Continued.

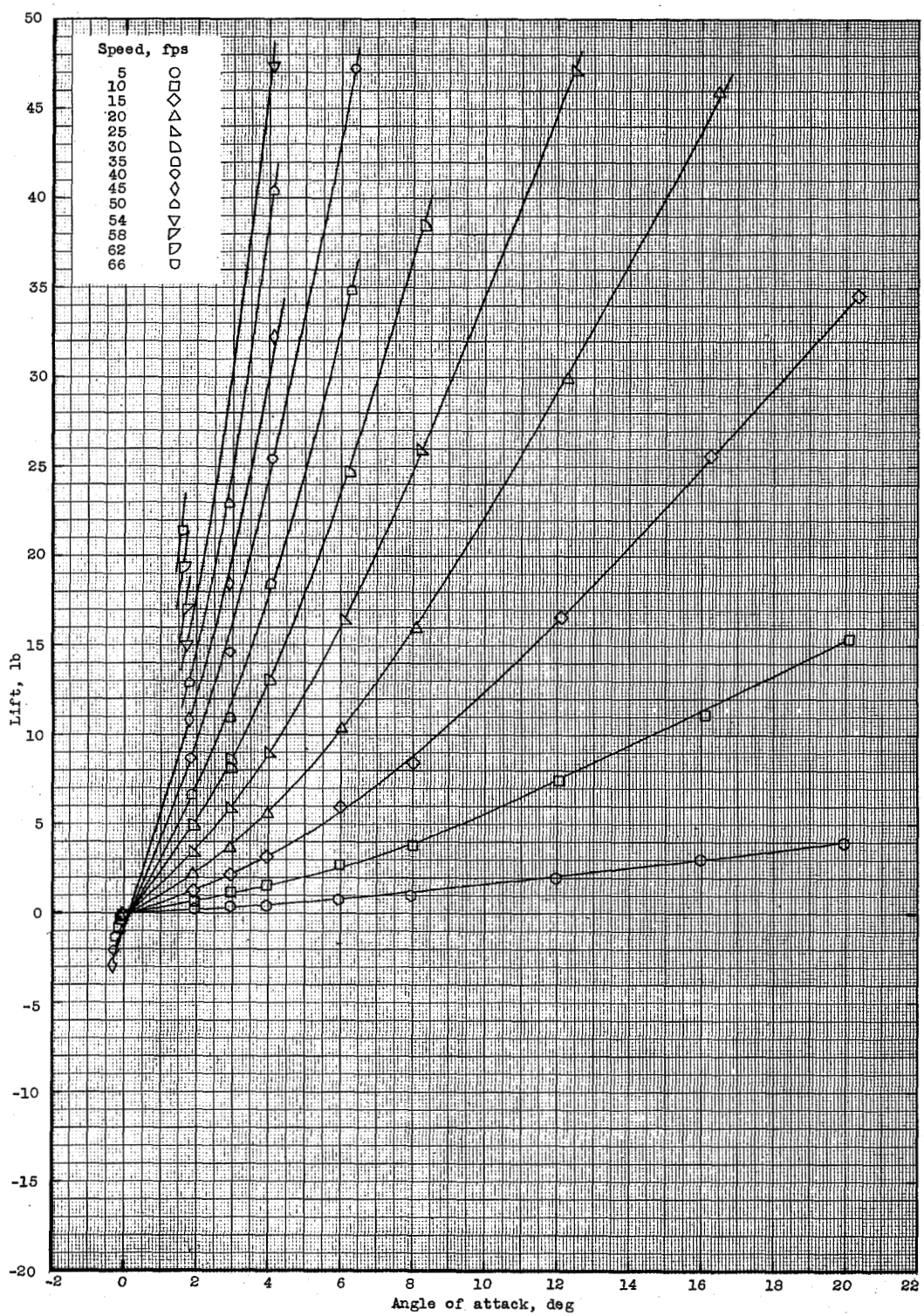

(c) Depth of submersion, 3.0 inches.

Figure 6.- Continued.

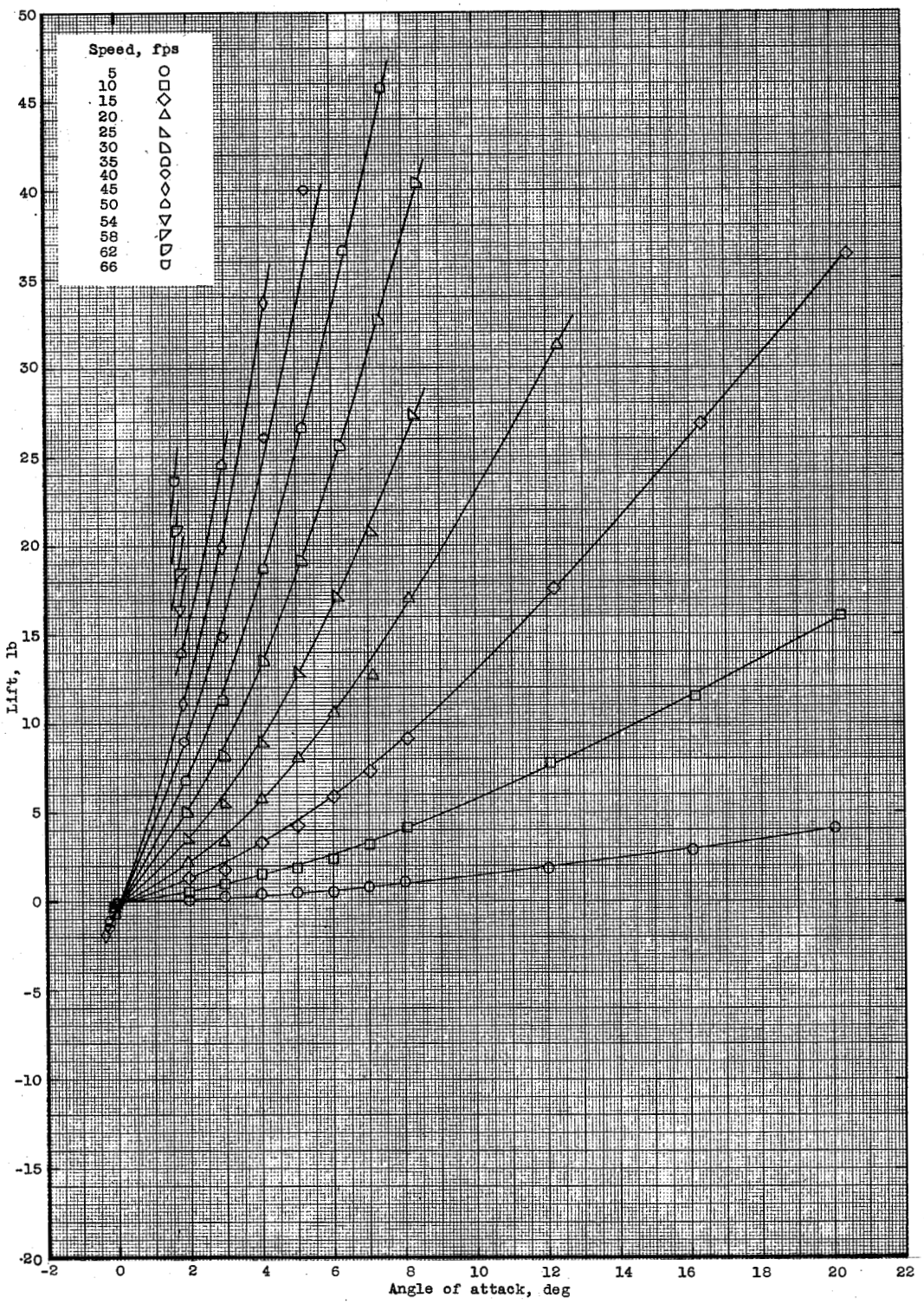

(d) Depth of submersion, 6.0 inches.

Figure 6.- Concluded.

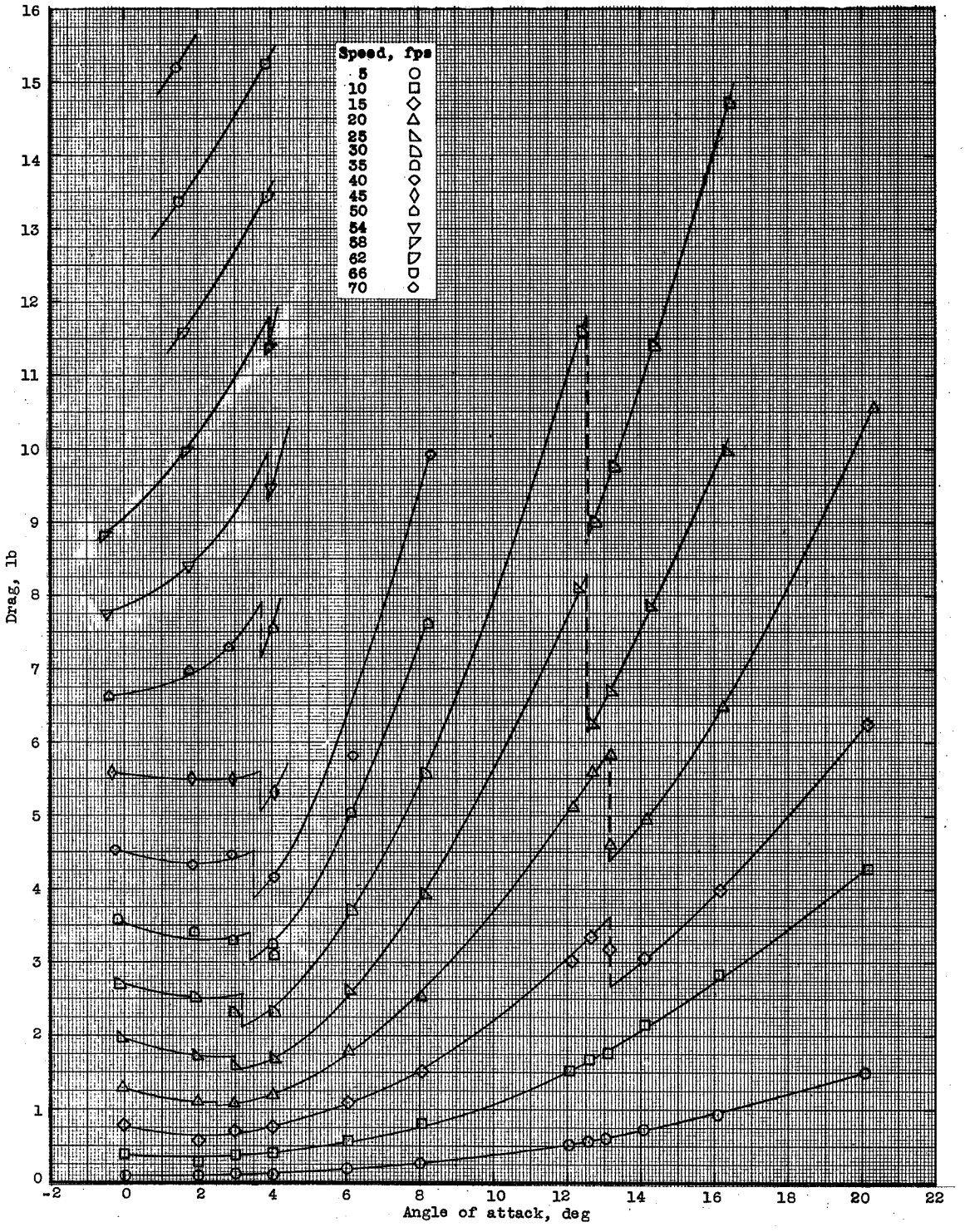

(a) Depth of submersion, 0.5 inch.

Figure 7.- Drag on the aspect-ratio-0.25 flat plate mounted on a single strut.

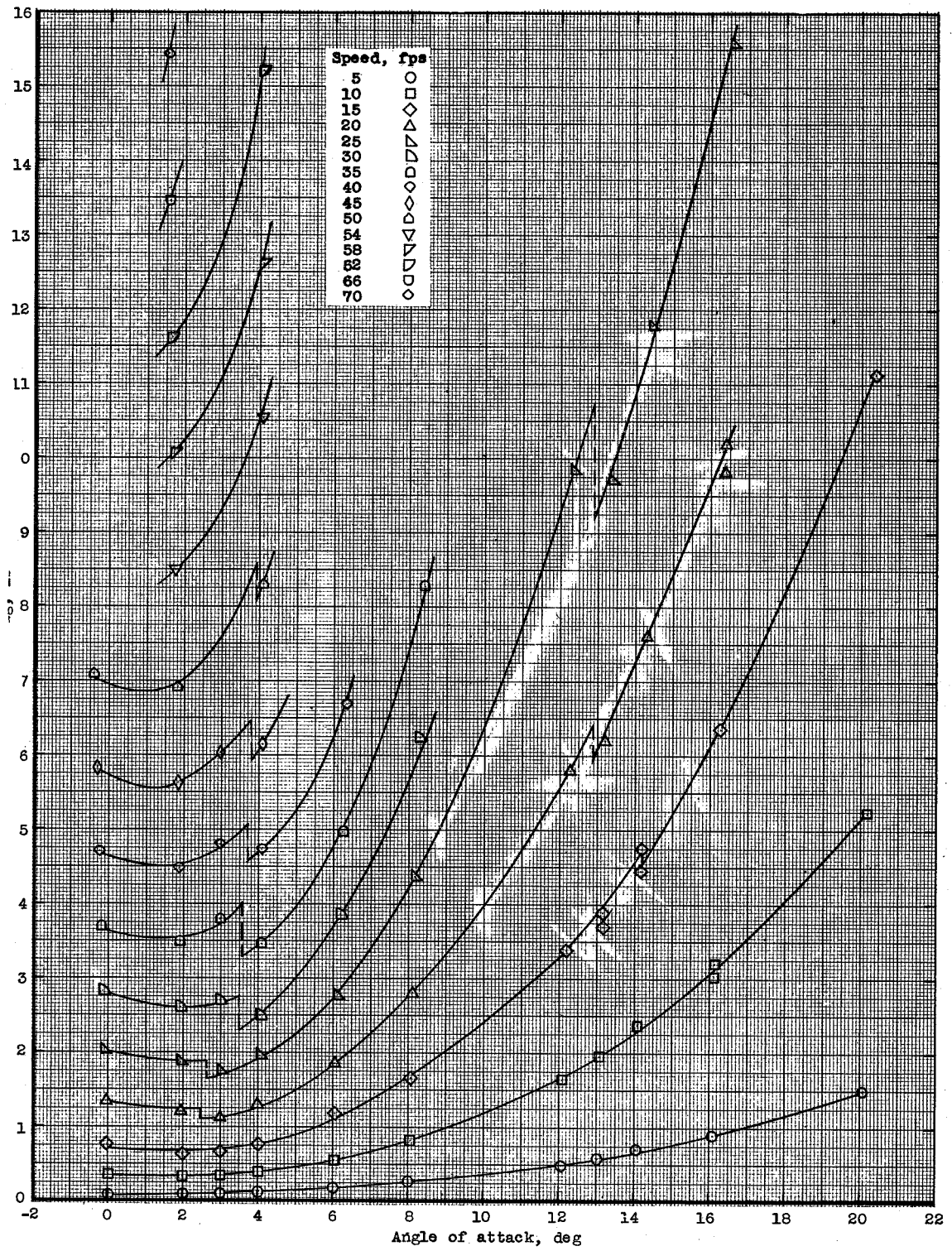

(b) Depth of submersion, 1.0 inch.

Figure 7.- Continued.

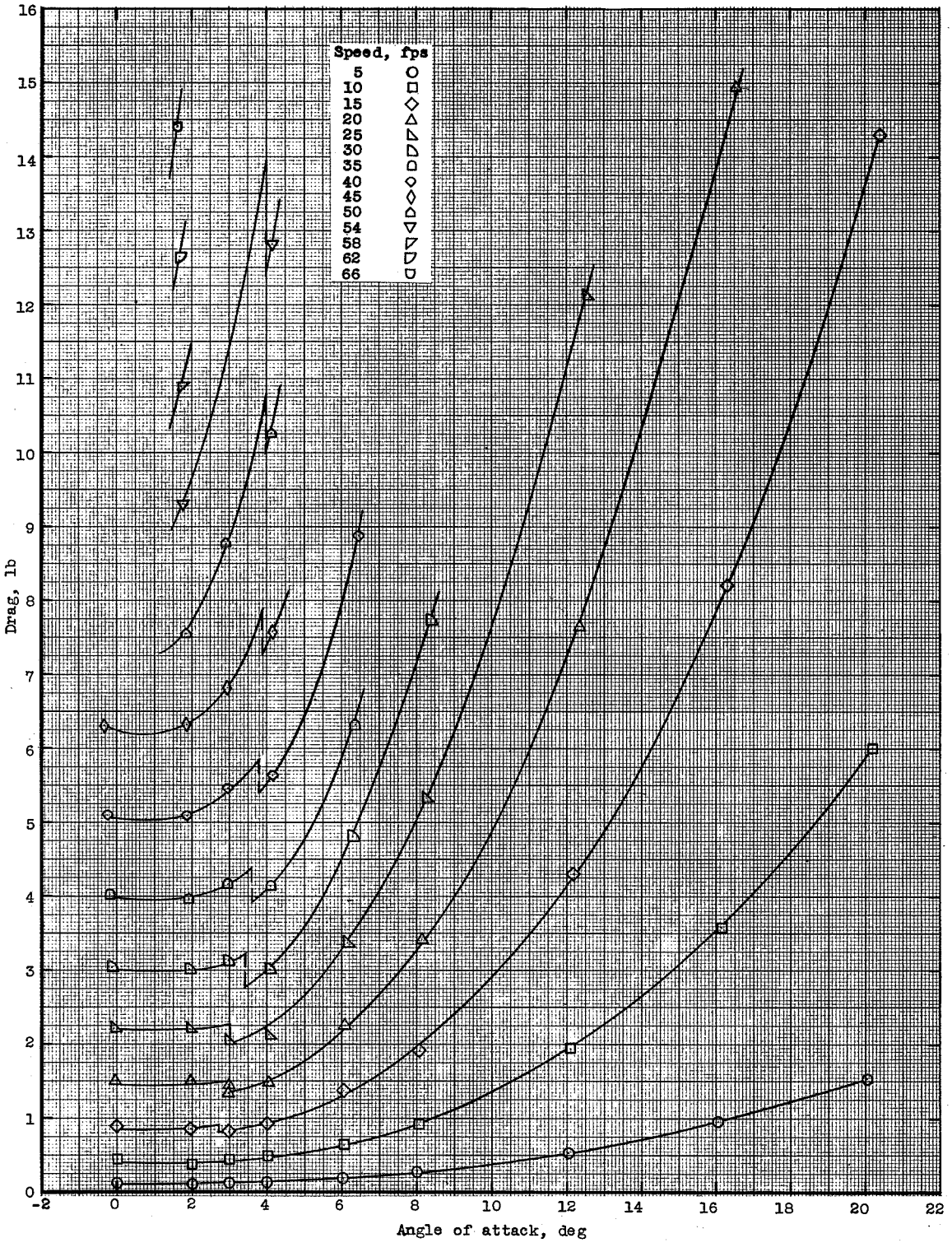

(c) Depth of submersion, 3.0 inches.

Figure 7.- Continued.

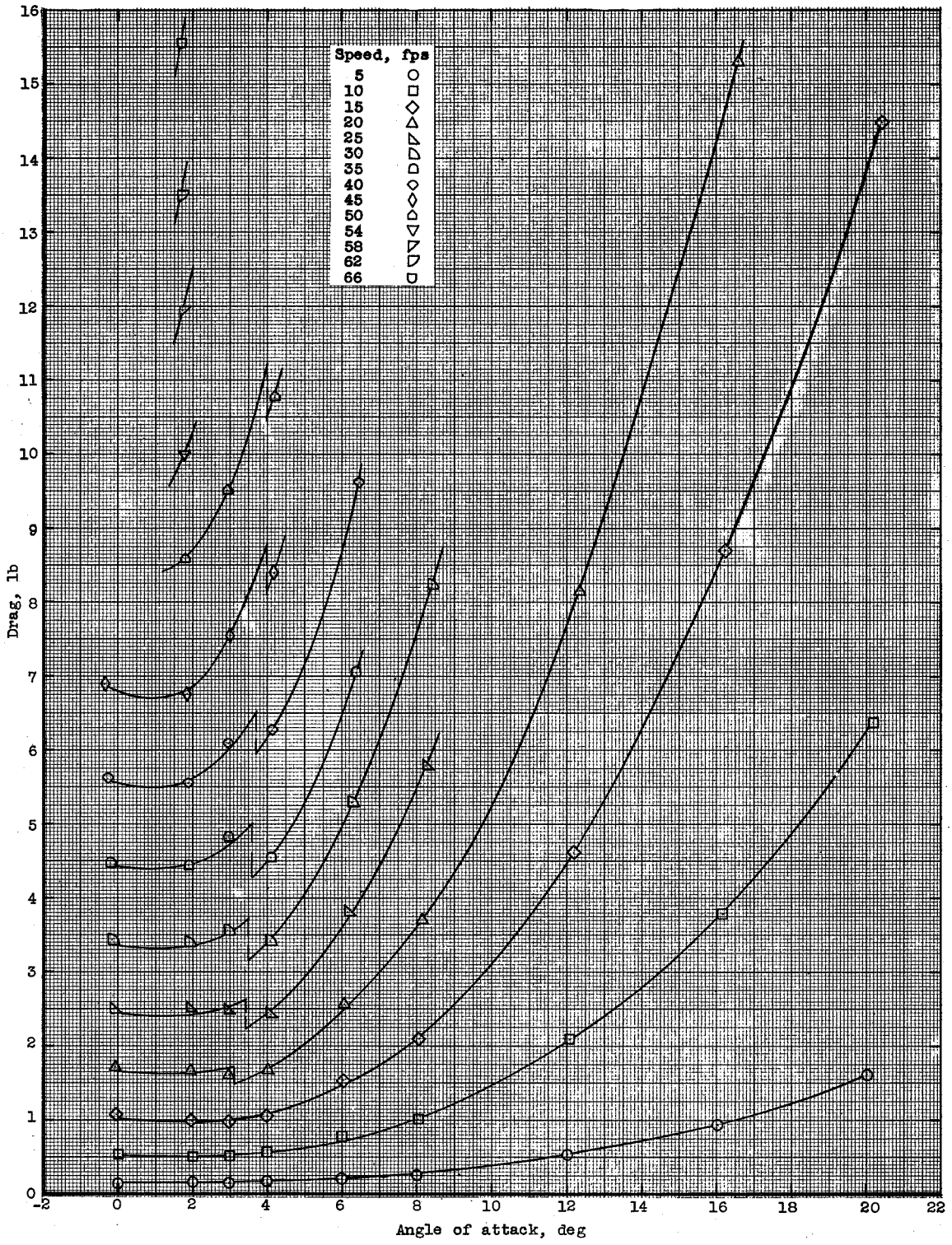

(d) Depth of submersion, 6.0 inches.

Figure 7.- Concluded.

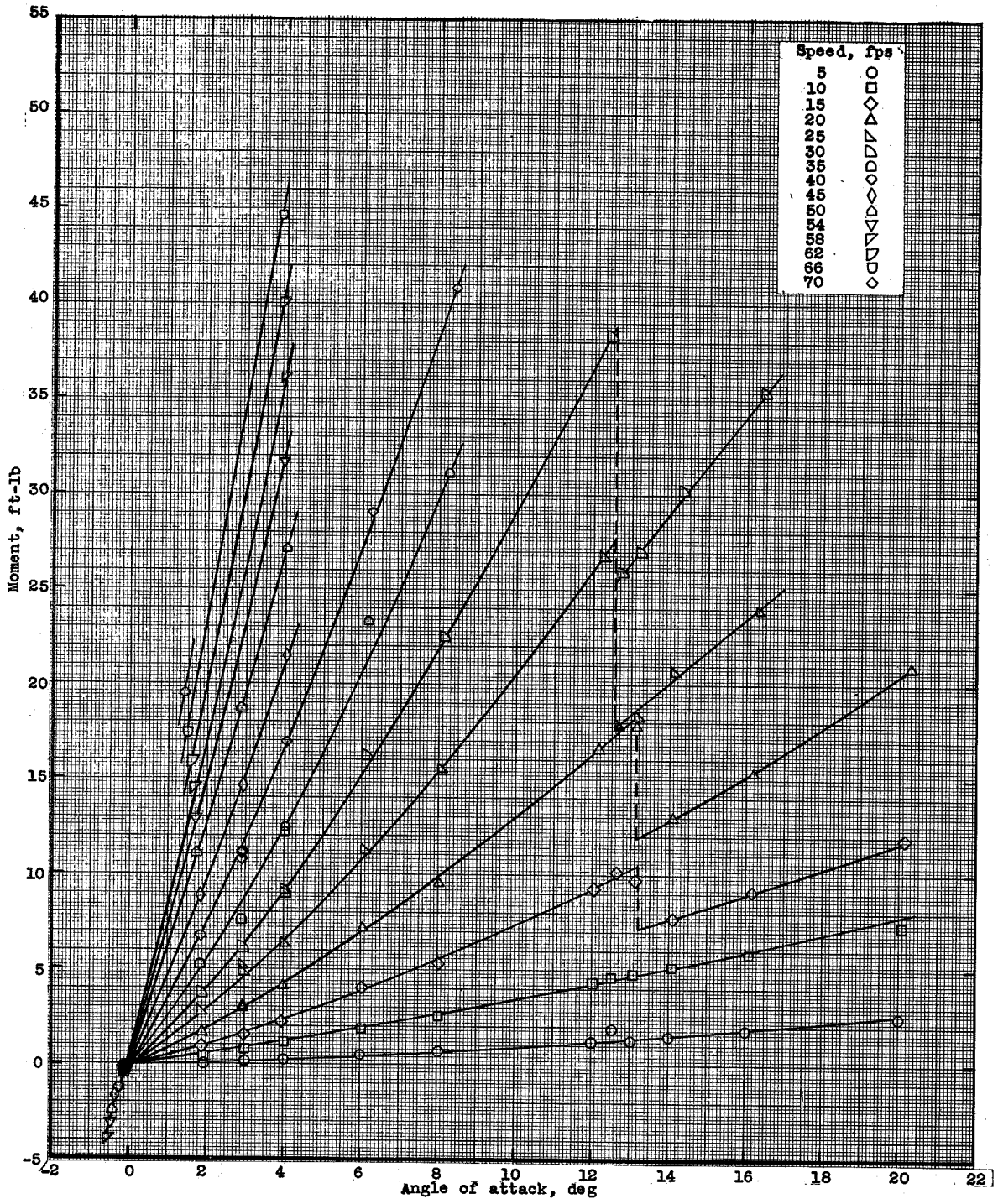

(a) Depth of submersion, 0.5 inch.

Figure 8.- Moment on the aspect-ratio-0.25 flat plate mounted on a single strut.

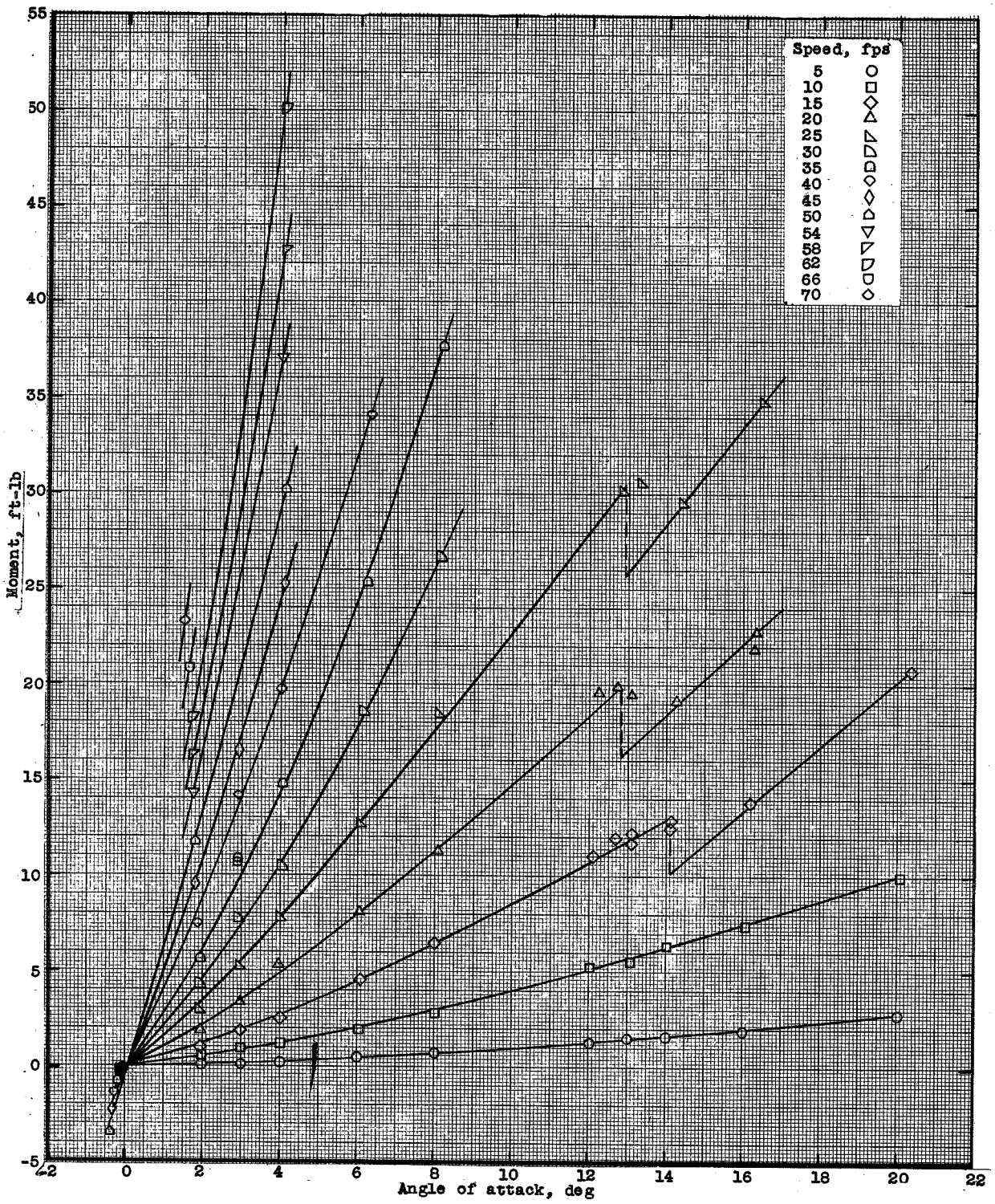

(b) Depth of submersion, 1.0 inch.

Figure 8.- Continued.

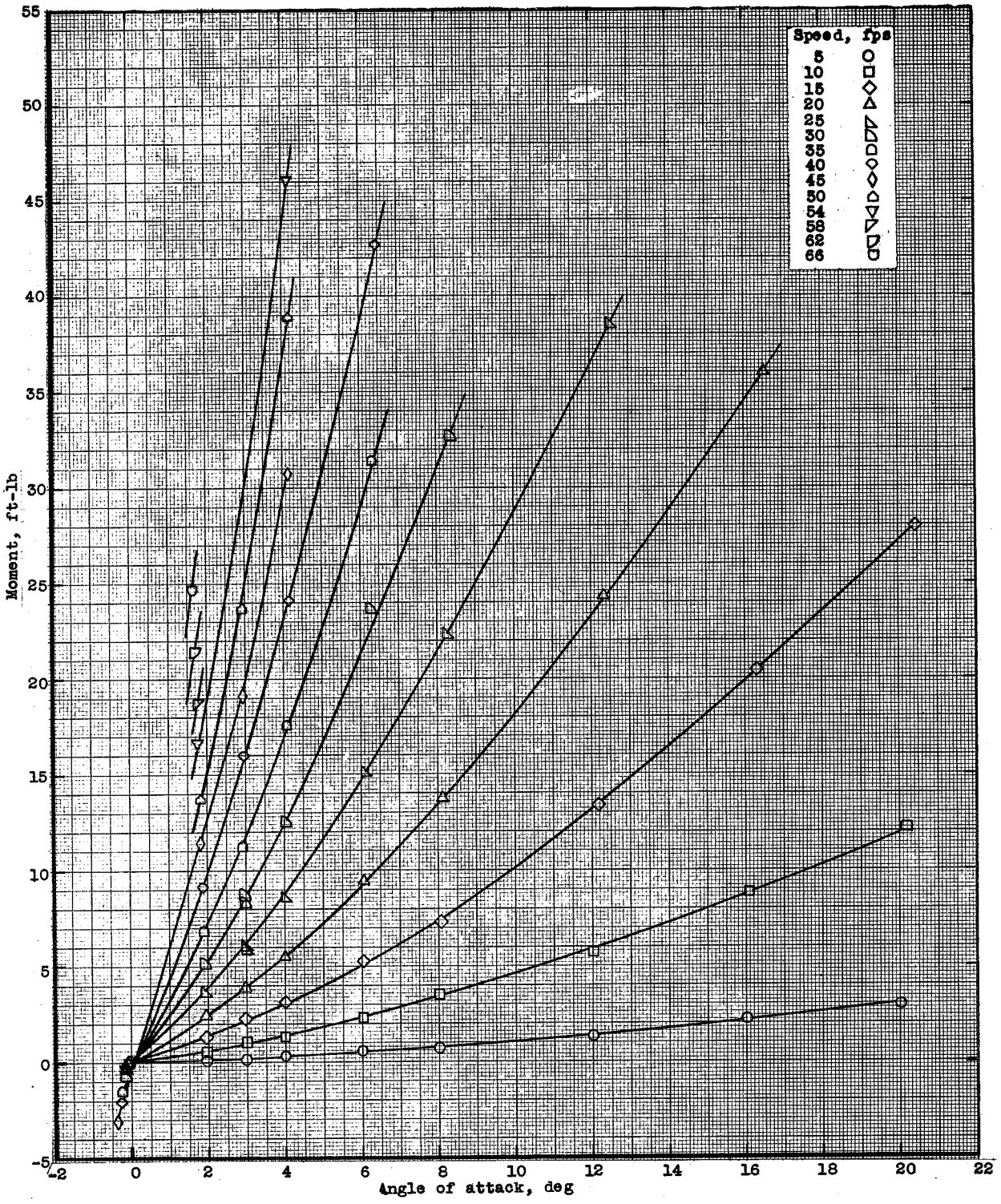

(c) Depth of submersion, 3.0 inches.

Figure 8.- Continued.

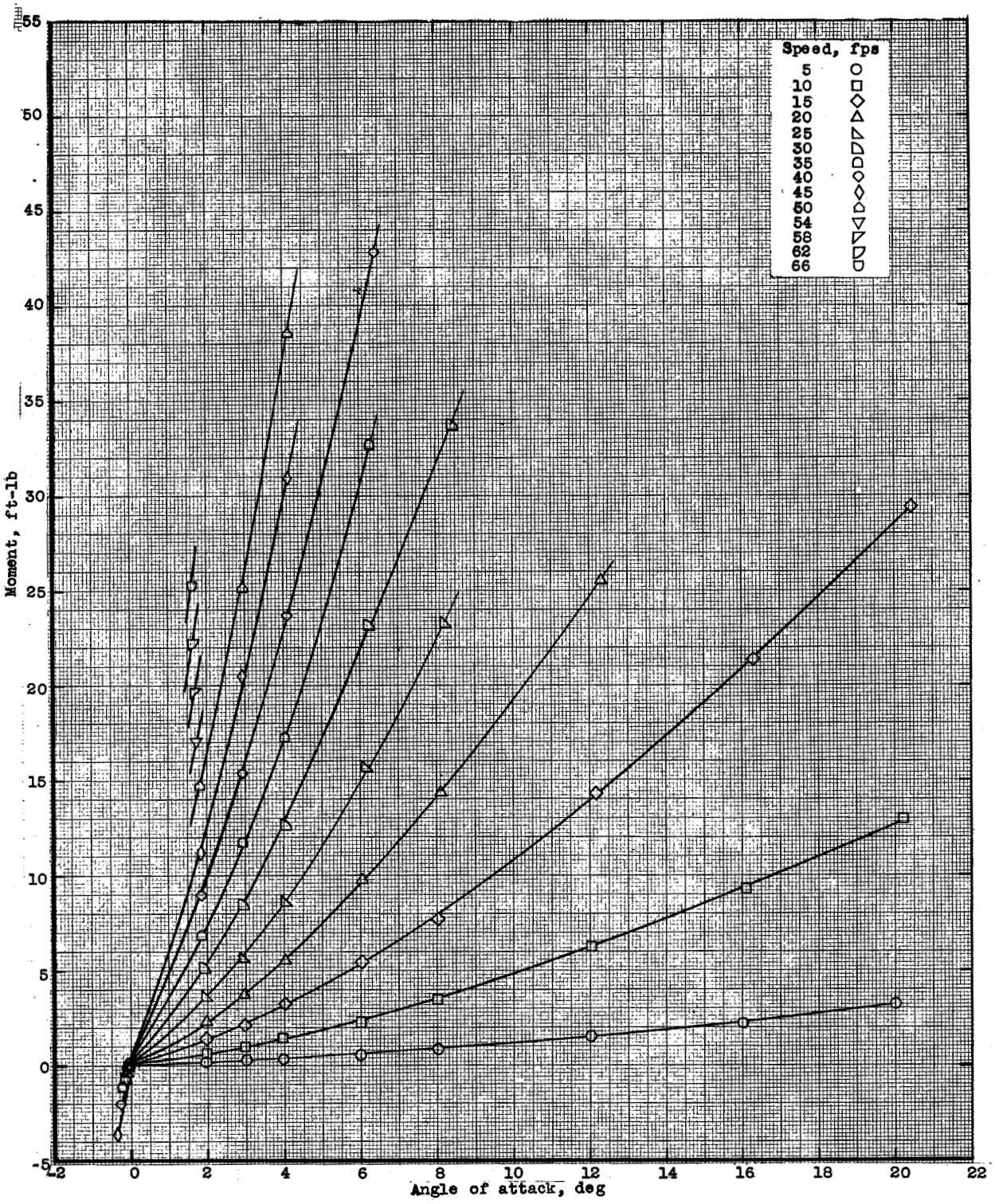

(d) Depth of submersion, 6.0 inches.

Figure 8.- Concluded.

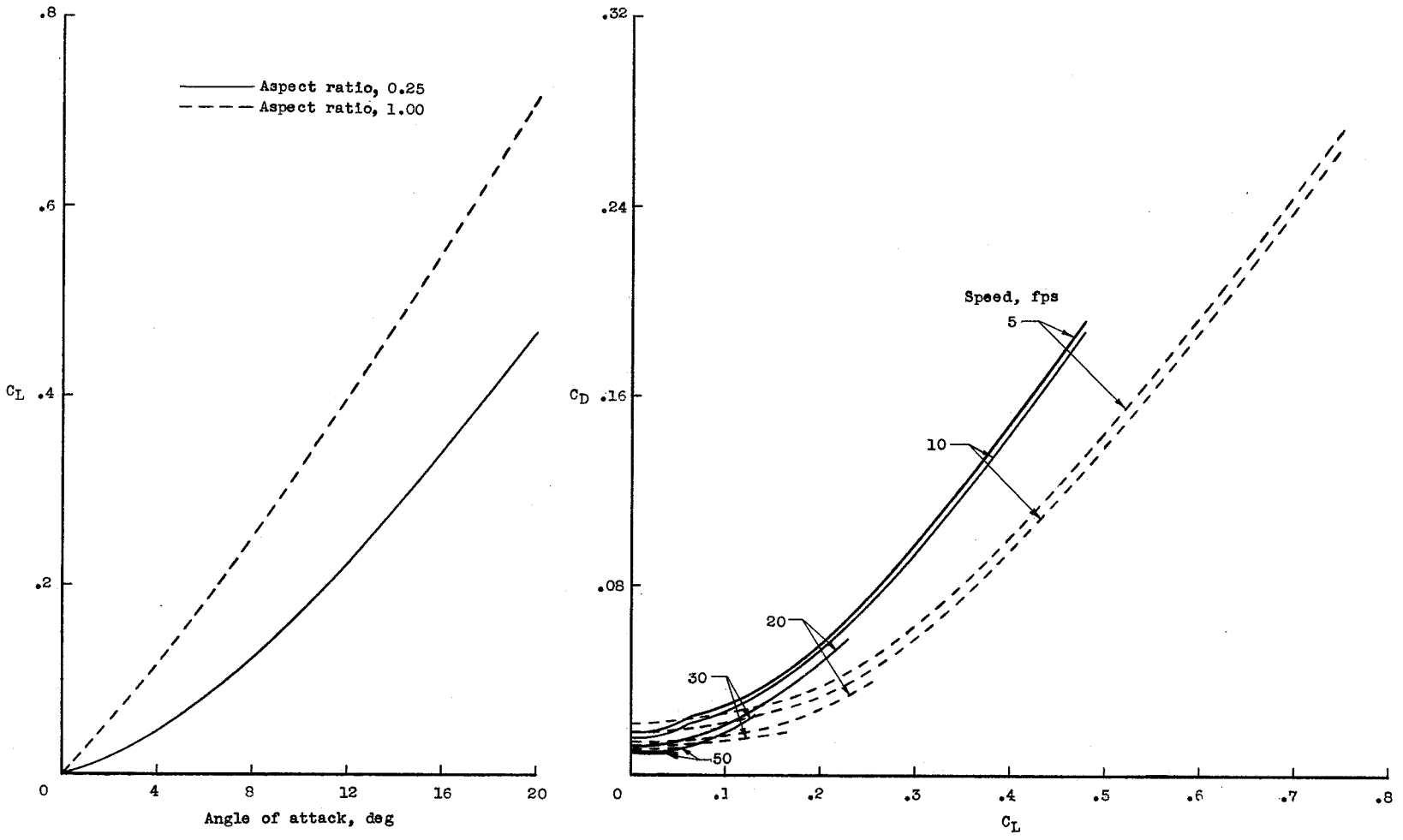

Figure 9.- The lift and drag characteristics for the aspect-ratio-1.00 and aspect-ratio-0.25 flat plates at a depth of 6.0 inches.

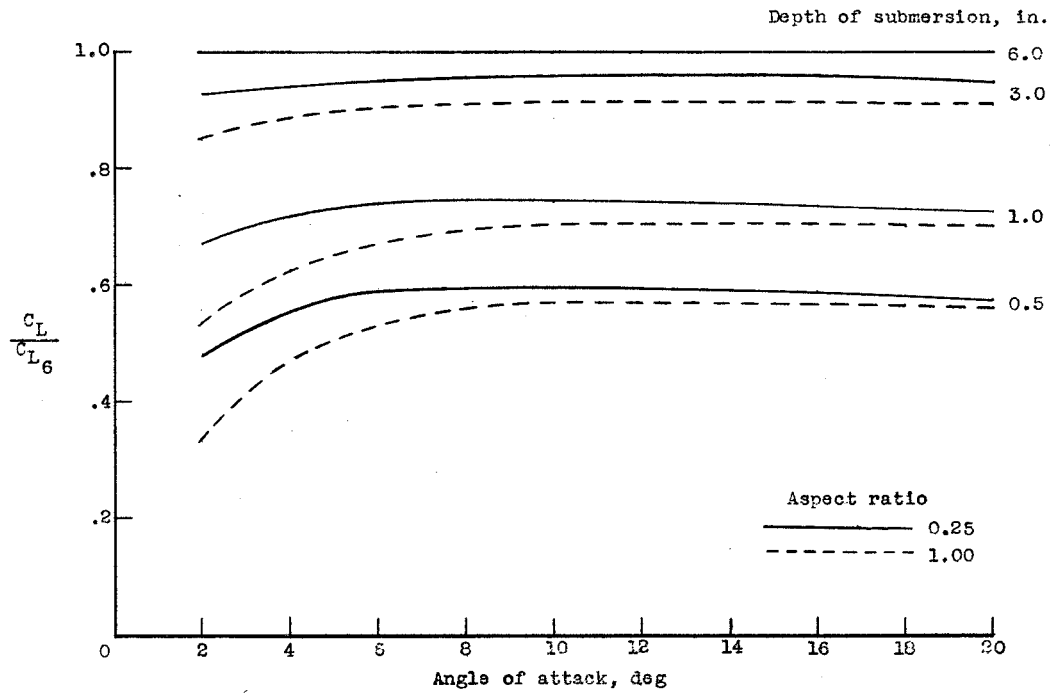

(a) Effect of angle of attack.

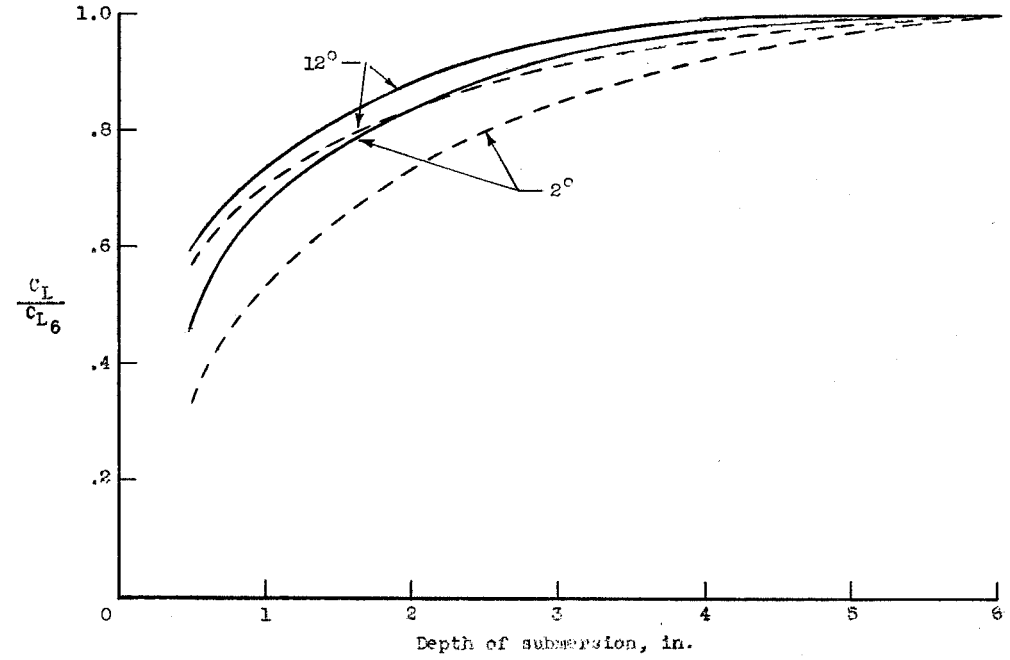

(b) Effect of depth of submersion.

Figure 10.- The variation of the lift characteristics with angle of attack and depth of submersion.

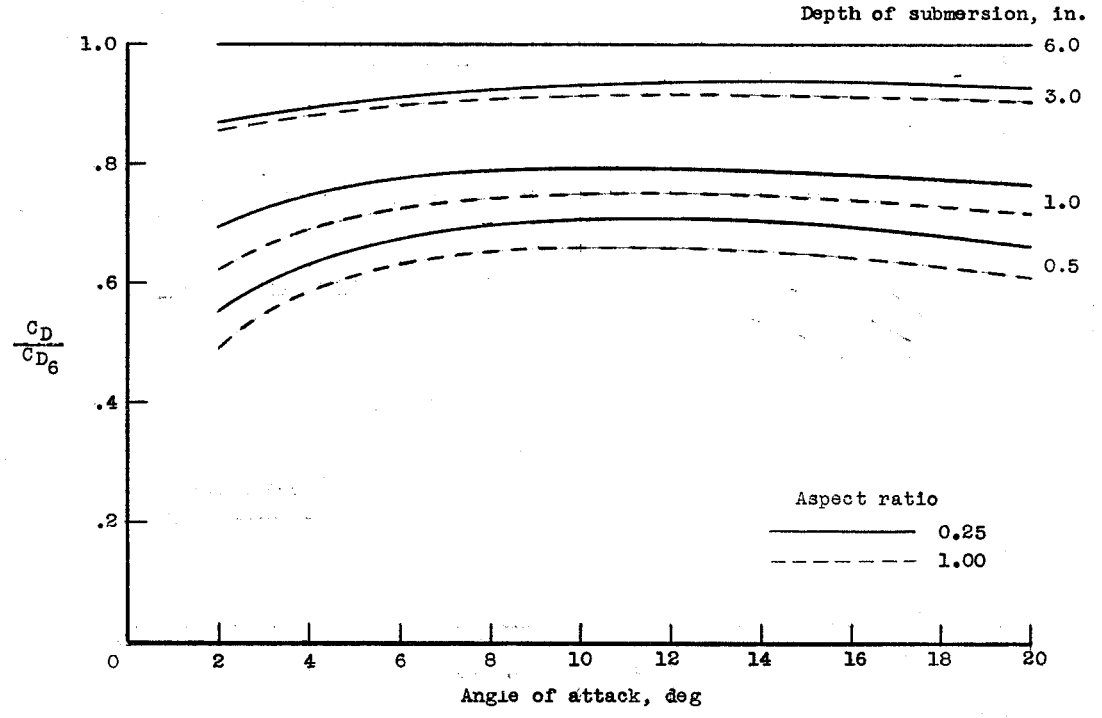

(a) Effect of angle of attack.

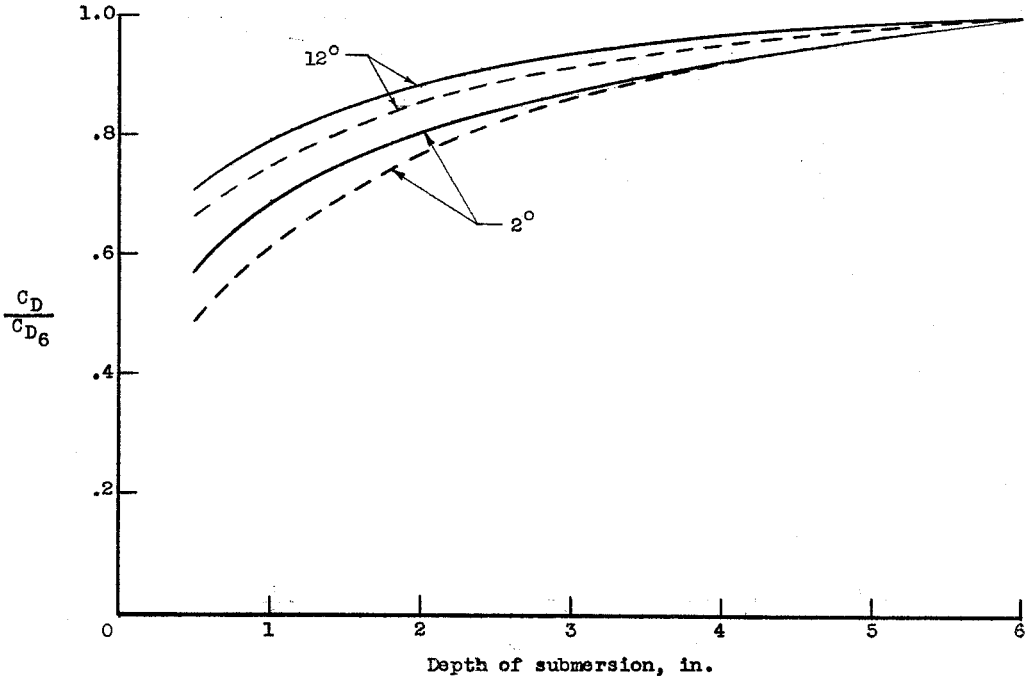

(b) Effect of depth of submersion.

Figure 11.- The variation of the drag characteristics with angle of attack and depth of submersion.

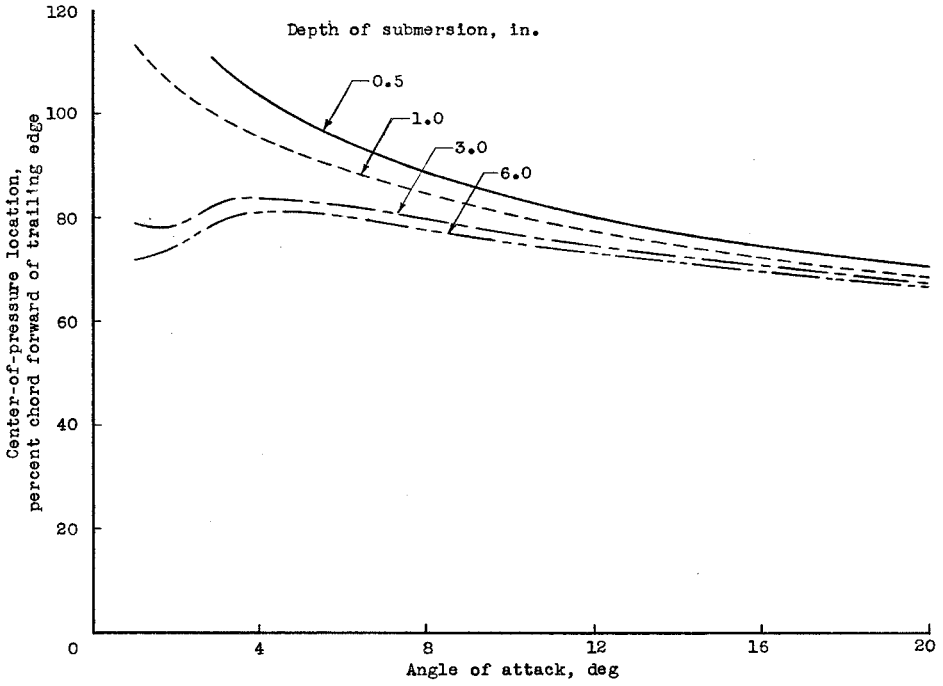

(a) Aspect ratio 1.00.

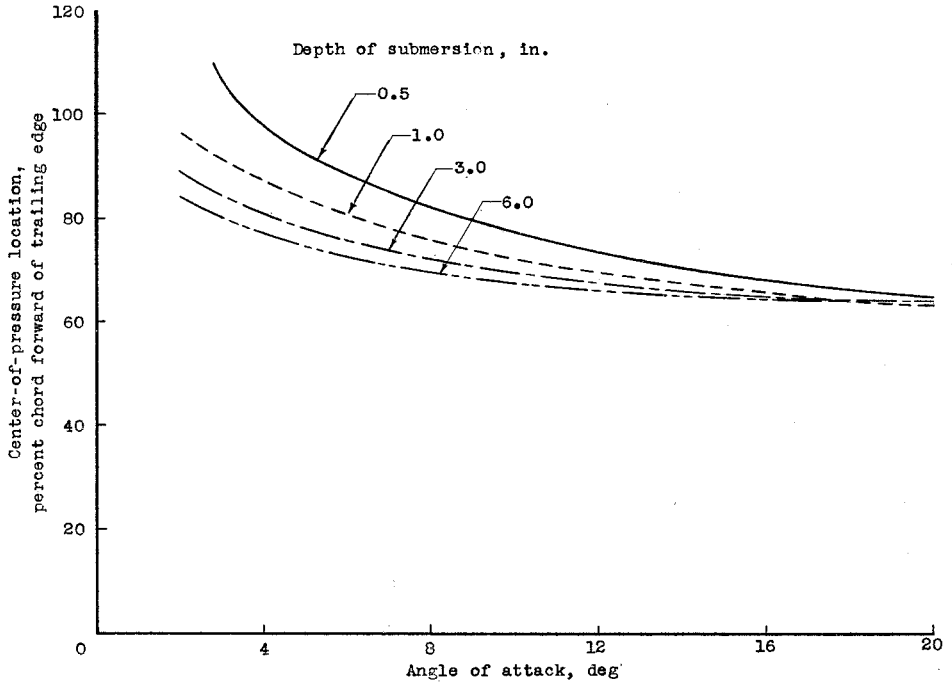

(b) Aspect ratio 0.25.

Figure 12.- The location of the center of pressure as a function of the angle of attack and the depth of submersion.

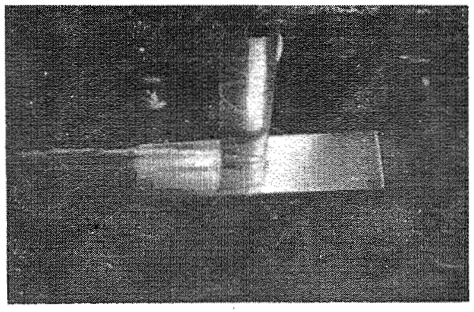

30 fps

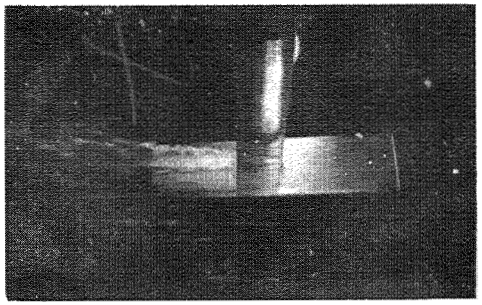

40 fps

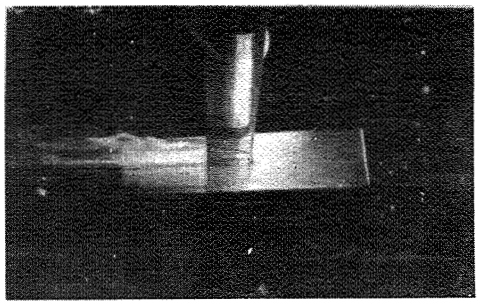

50 fps

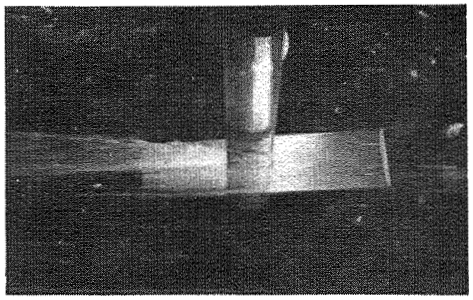

54 fps

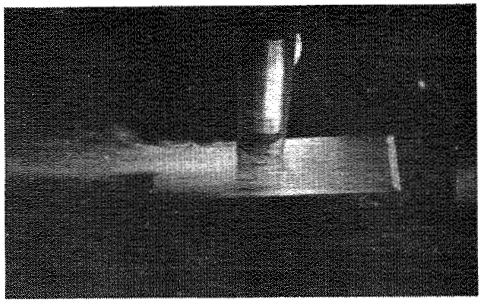

62 fps

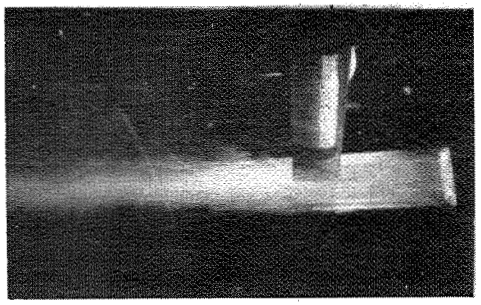

70 fps

L-82091

Figure 13.- Sequence photographs of a typical run showing the formation of cavitation for the aspect-ratio-0.25 flat plate. (Angle of attack, 2°; depth of submersion, 0.5 inch.)

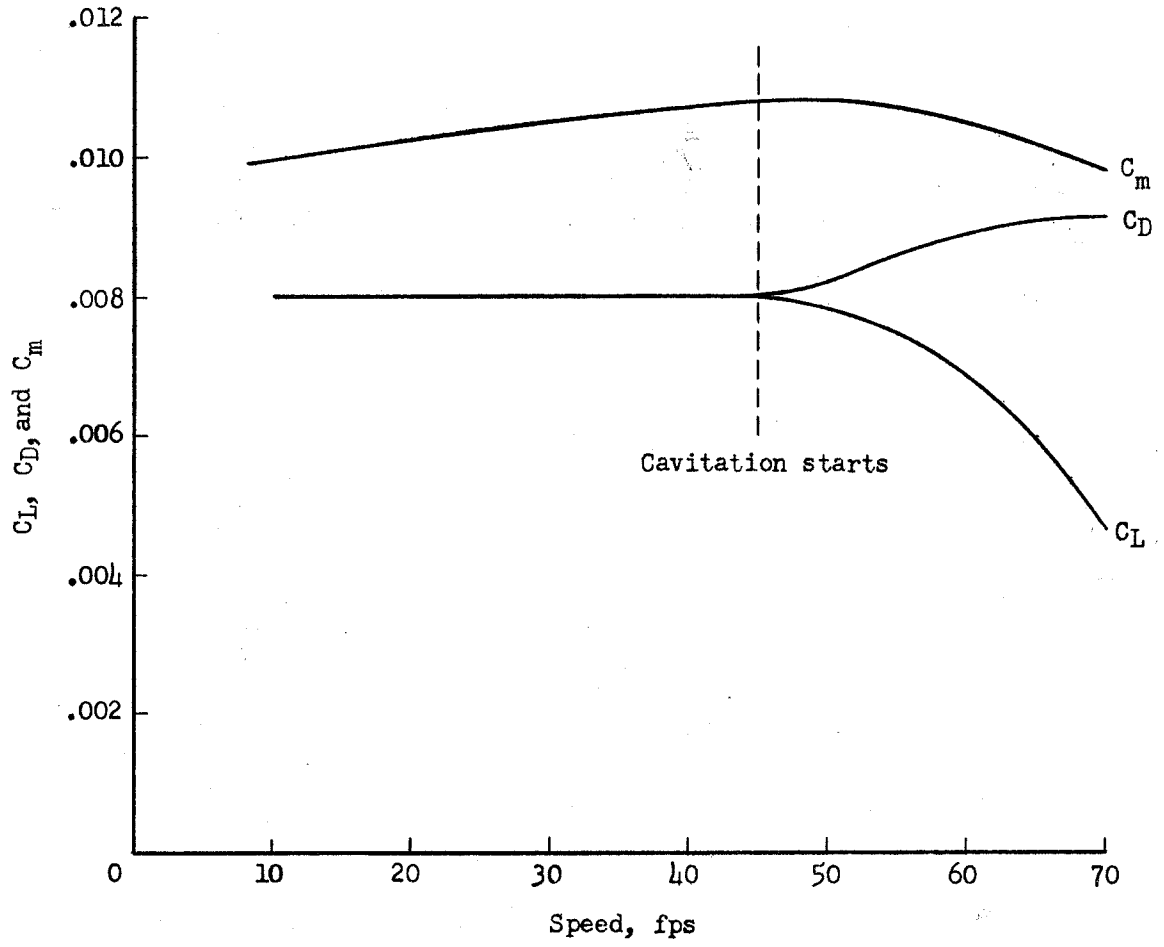

Figure 14.- Effect of the formation of cavitation on the force and moment characteristics for the aspect-ratio-0.25 flat plate. (Angle of attack, 2°; depth of submersion, 0.5 inch.)

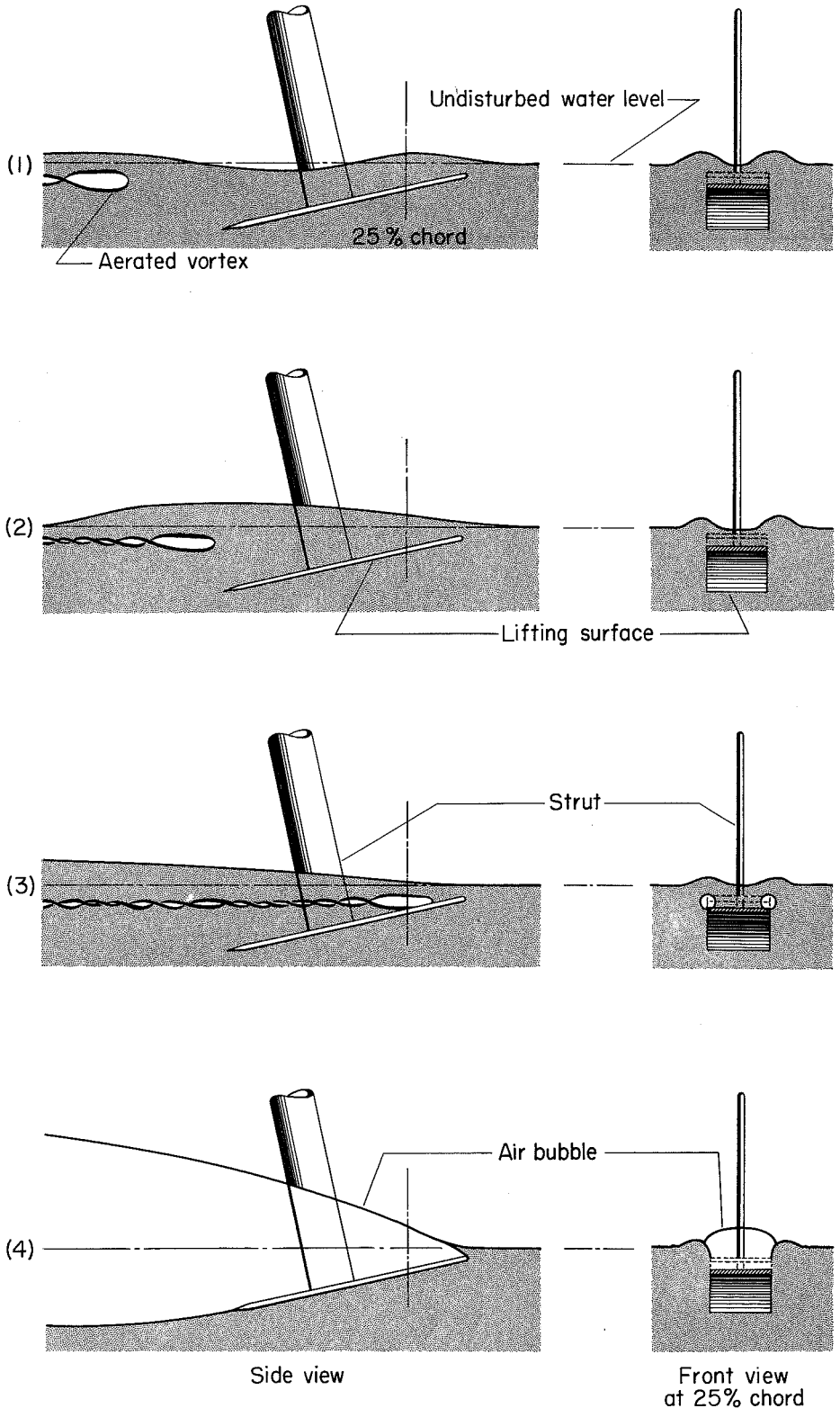

Figure 15.- Schematic drawing depicting development of ventilation.

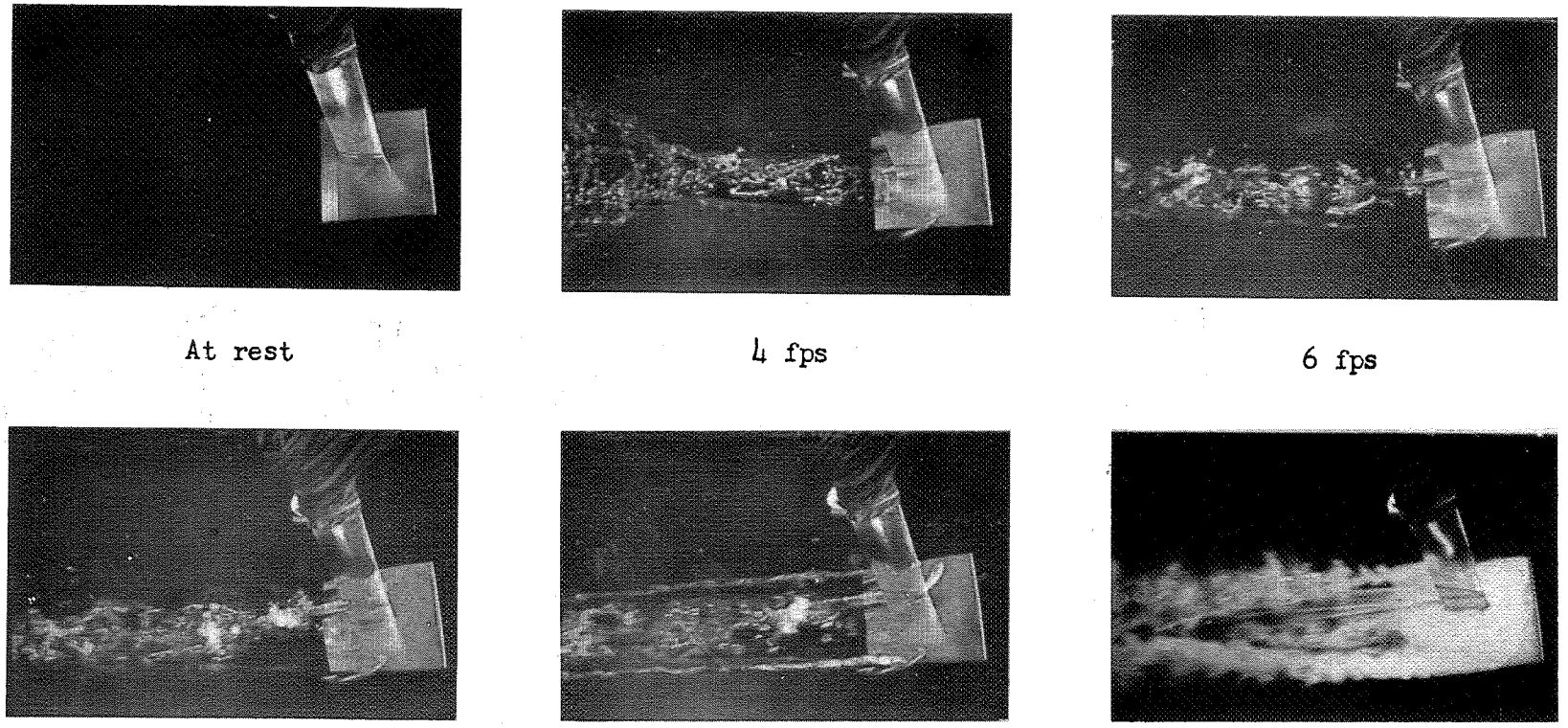

At rest | 4 fps | 6 fps

8 fps | 10 fps | 12.5 fps

L-82092

Figure 16.- Sequence photographs of a typical run showing the formation of "white water" for the aspect-ratio-1.00 flat plate. (Angle of attack, 16°; depth of submersion, 1.0 inch.)

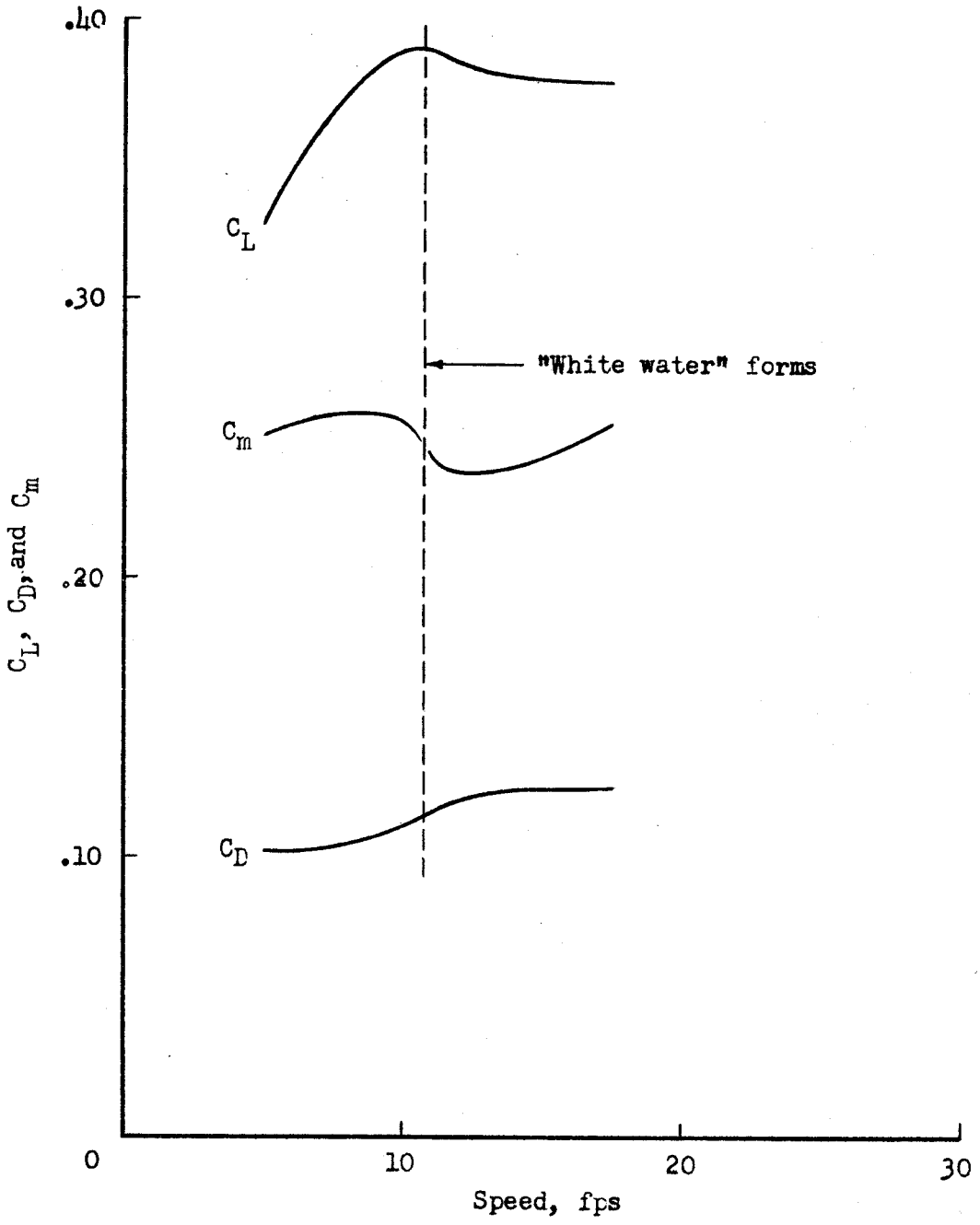

Figure 17.- Effect of the formation of "white water" on the force and moment characteristics of the aspect-ratio-1.00 flat plate. (Angle of attack, 16°; depth of submersion, 1.0 inch.)

5 fps

10 fps

12 fps

13 fps

15 fps

25 fps

L-82093

Figure 18.- Sequence photographs of a typical run showing the formation of the "planing bubble" for the aspect-ratio-1.00 flat plate. (Angle of attack, 12°; depth of submersion, 0.5 inch.)

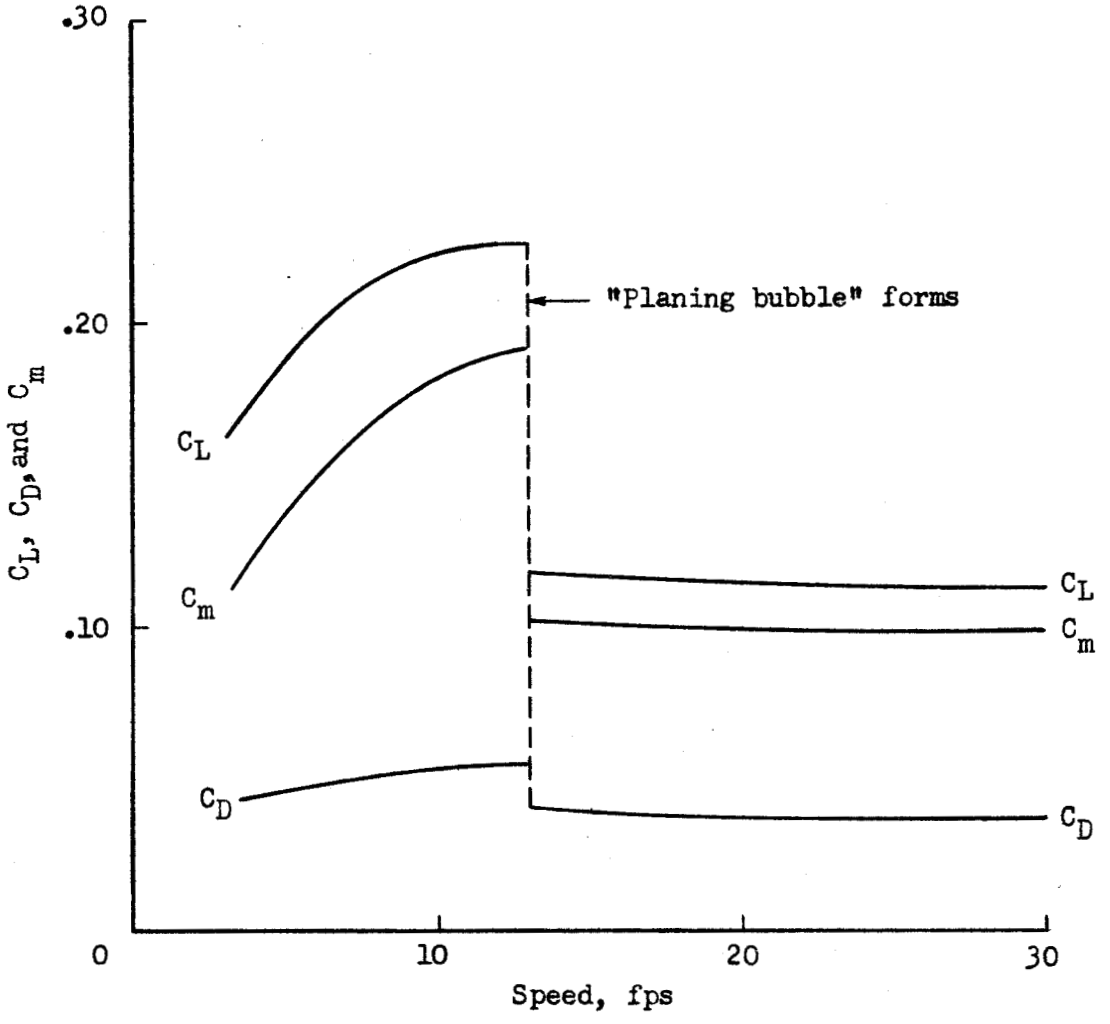

Figure 19.- Effect of the formation of the "planing bubble" on the force and moment characteristics of the aspect-ratio-1.00 flat plate. (Angle of attack, 12°; depth of submersion, 0.5 inch.)

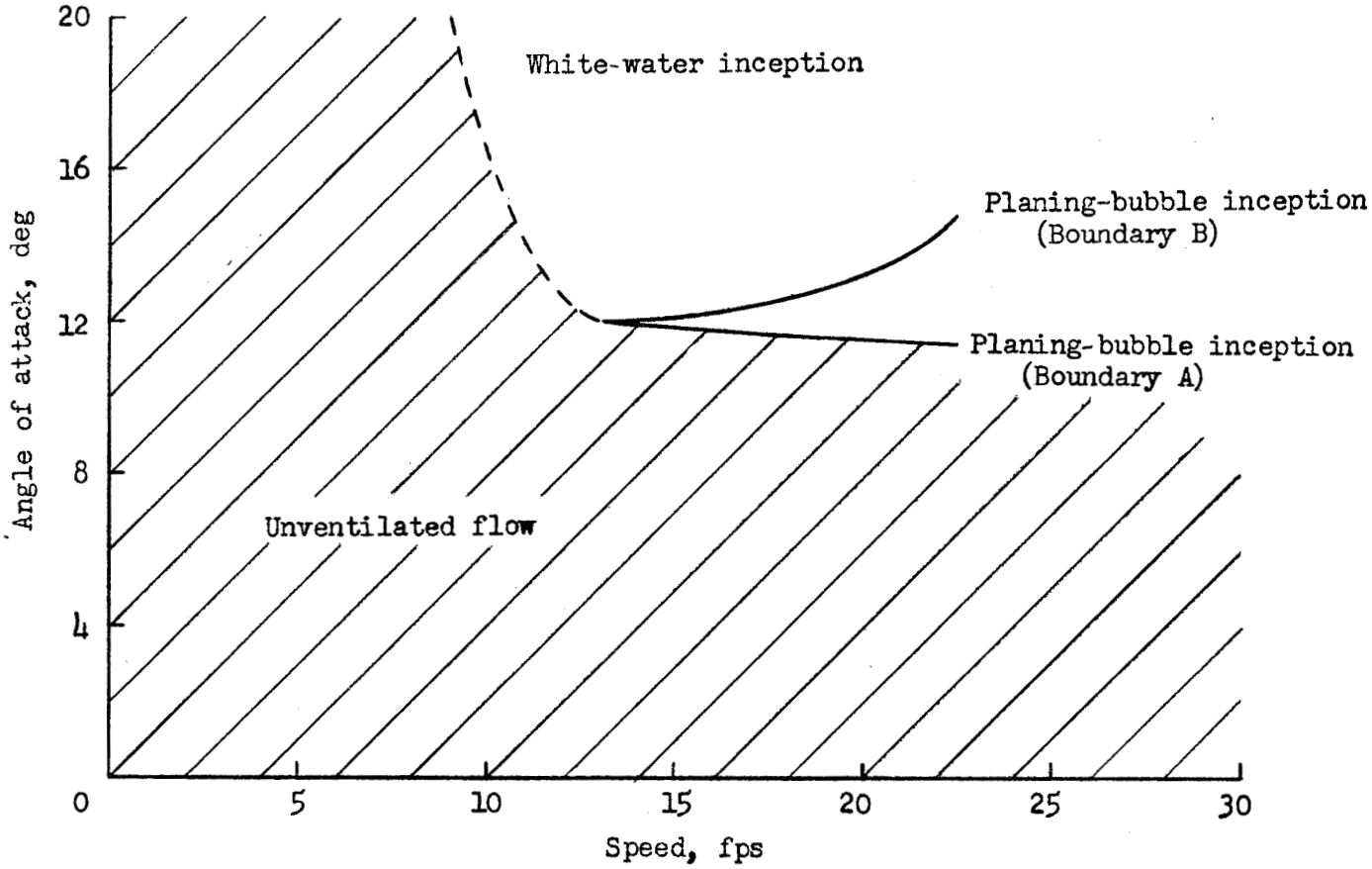

Figure 20.- Ventilation boundaries for the aspect-ratio-1.00 plate at a depth of submersion of 0.5 inch.

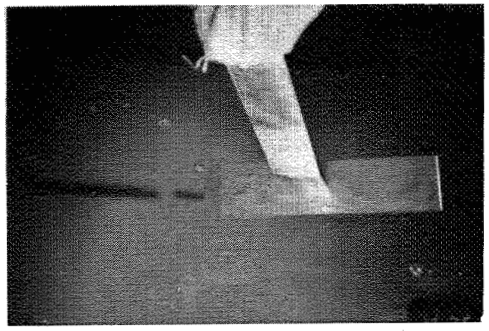

At rest

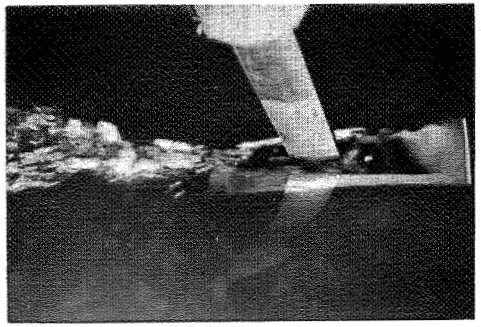

5 fps

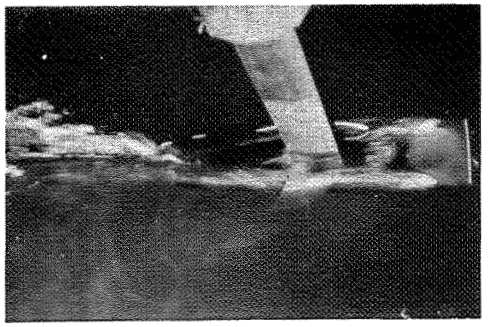

10 fps

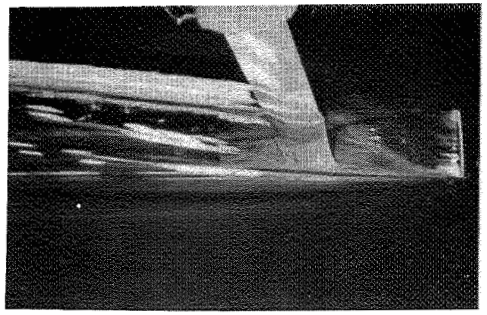

15 fps

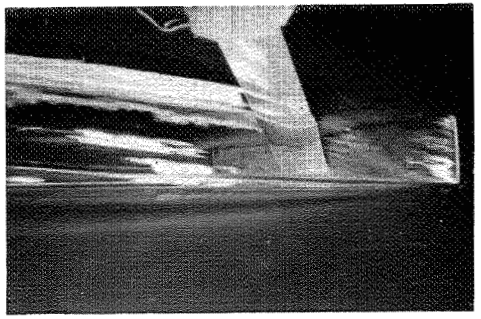

20 fps

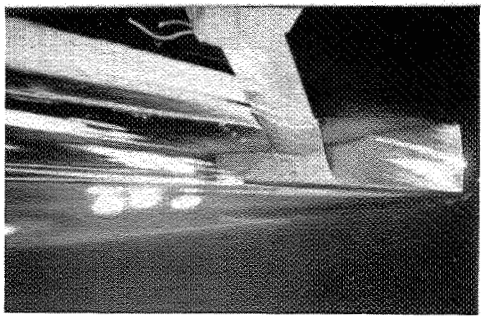

30 fps

L-82094

Figure 21.- Sequence photographs of a typical run showing the formation of the "planing bubble" for the aspect-ratio-0.25 flat plate. (Angle of attack, 16°; depth of submersion, 0.5 inch.)

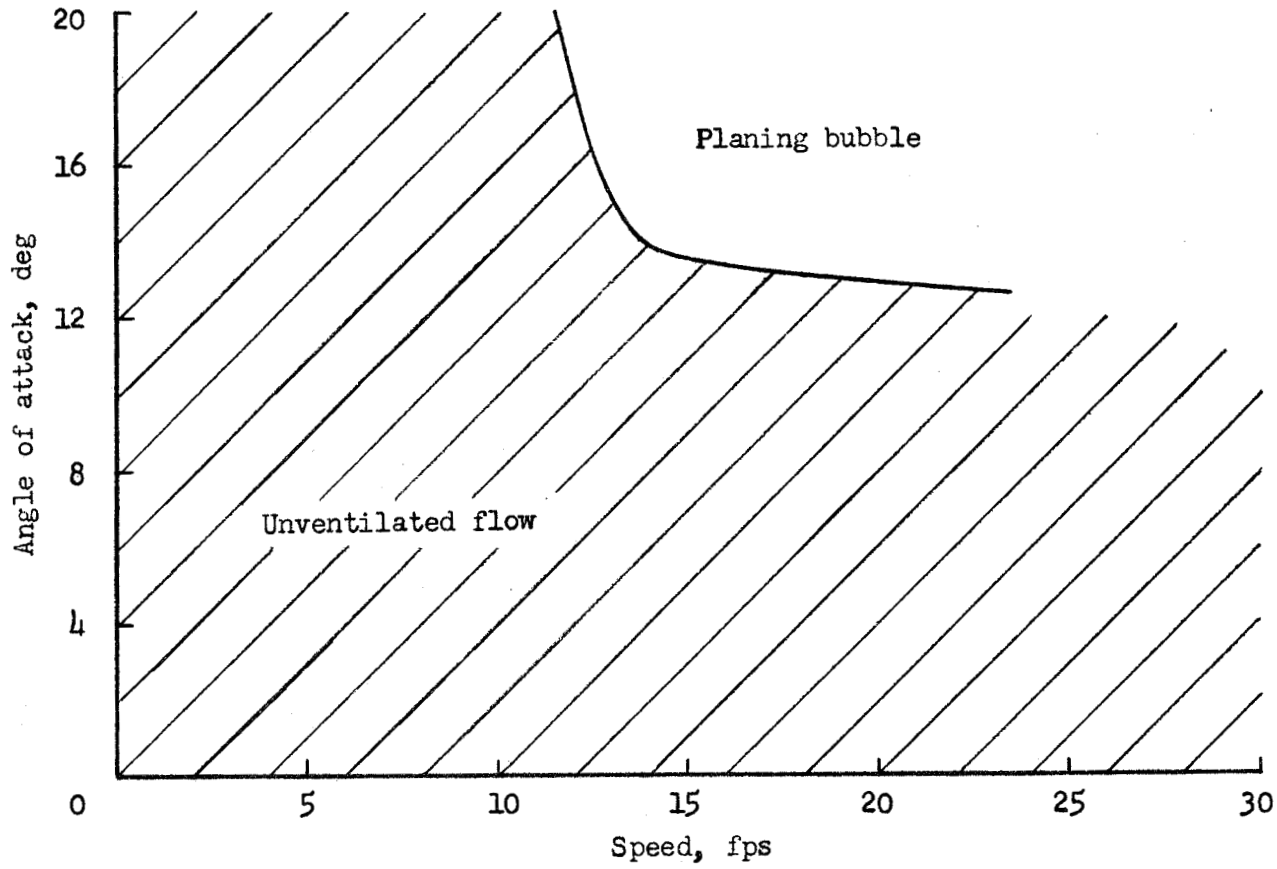

Figure 22.- Ventilation boundaries for the aspect-ratio-0.25 plate at a depth of submersion of 0.5 inch.

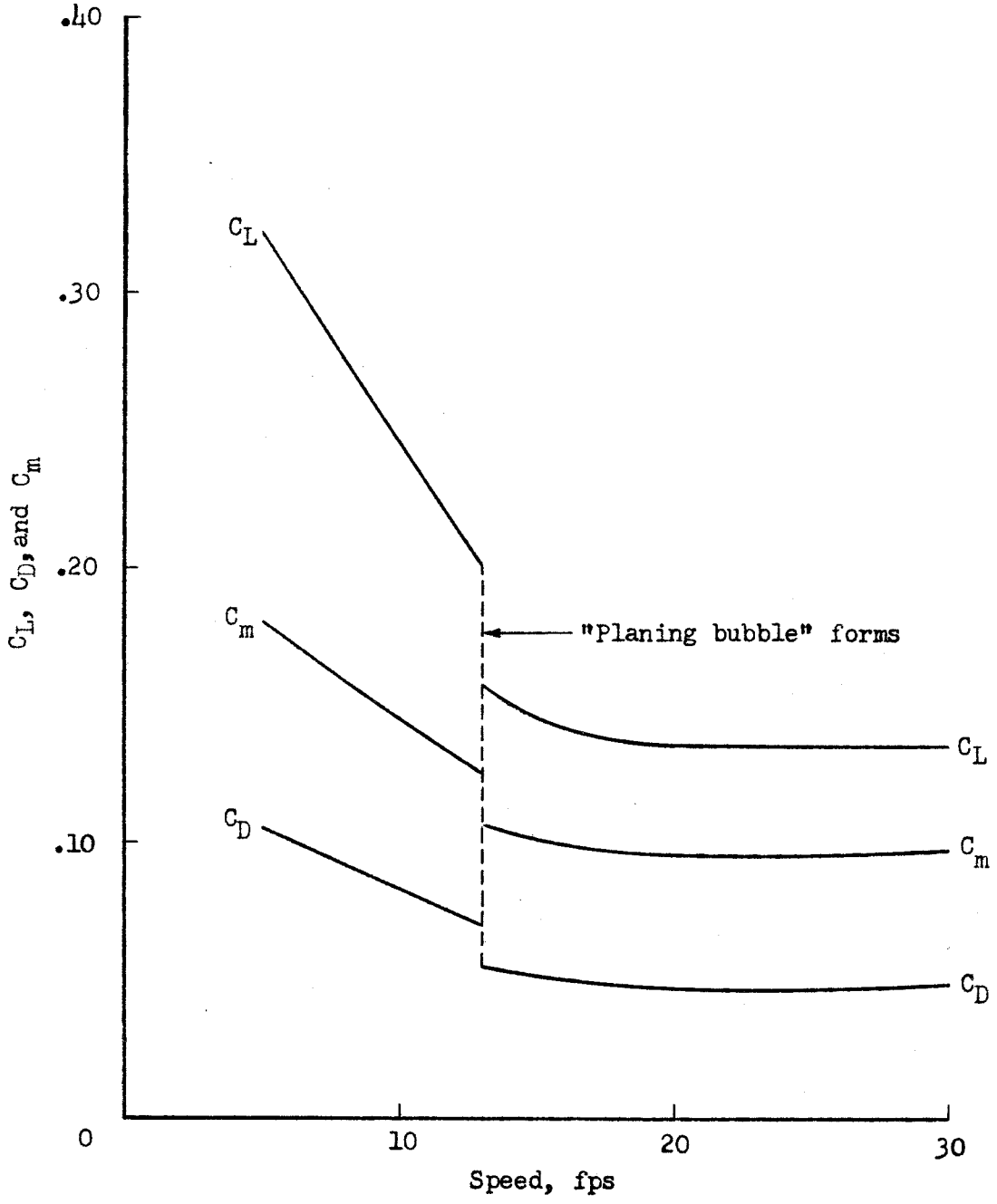

Figure 23.- Effect of the formation of the "planing bubble" on the force and moment characteristics for the aspect-ratio-0.25 flat plate. (Angle of attack, 16°; depth of submersion, 0.5 inch.)

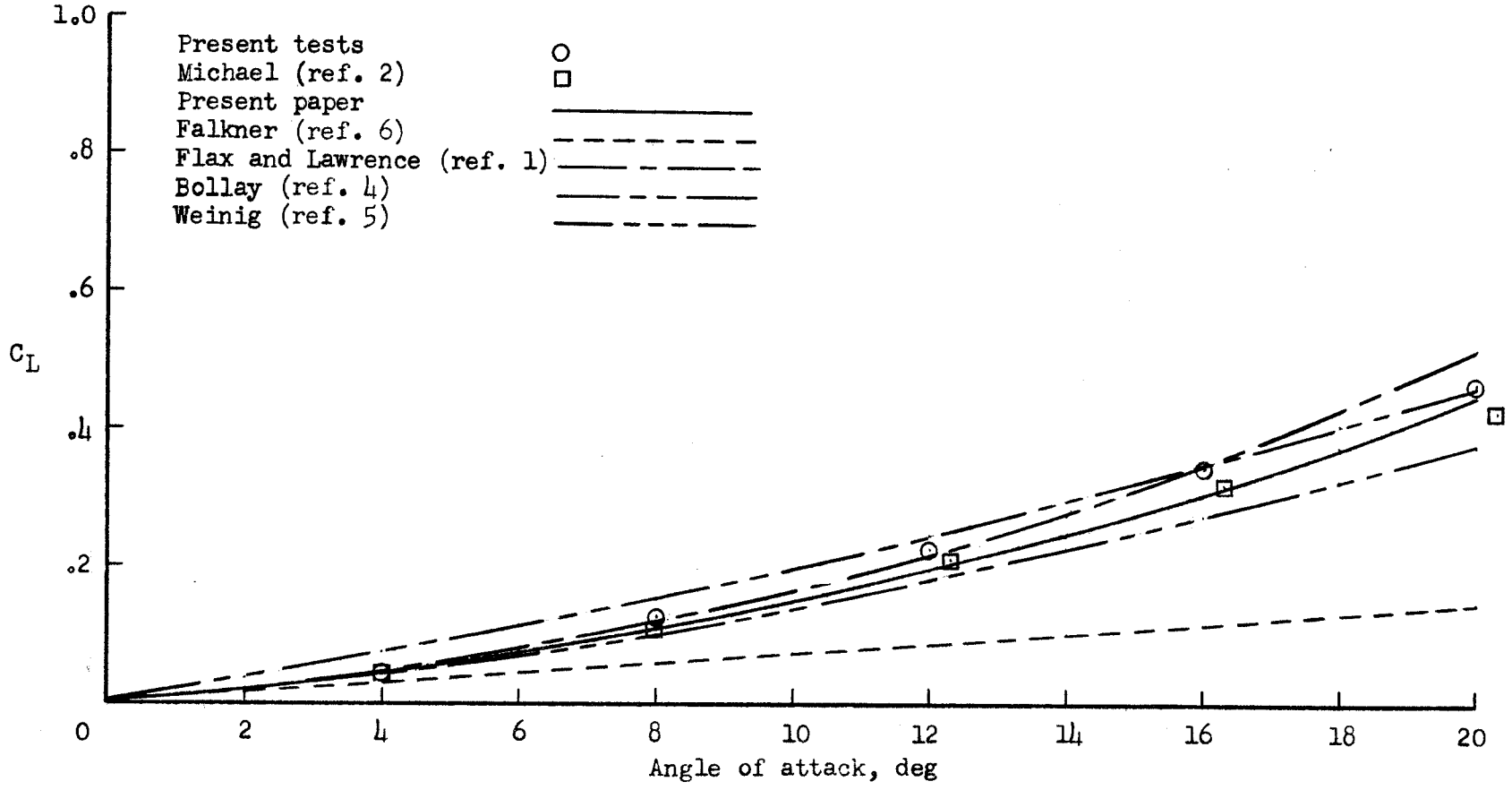

Figure 24.- Comparison between experimental and theoretical lift coefficients for aspect-ratio-0.25 surface.

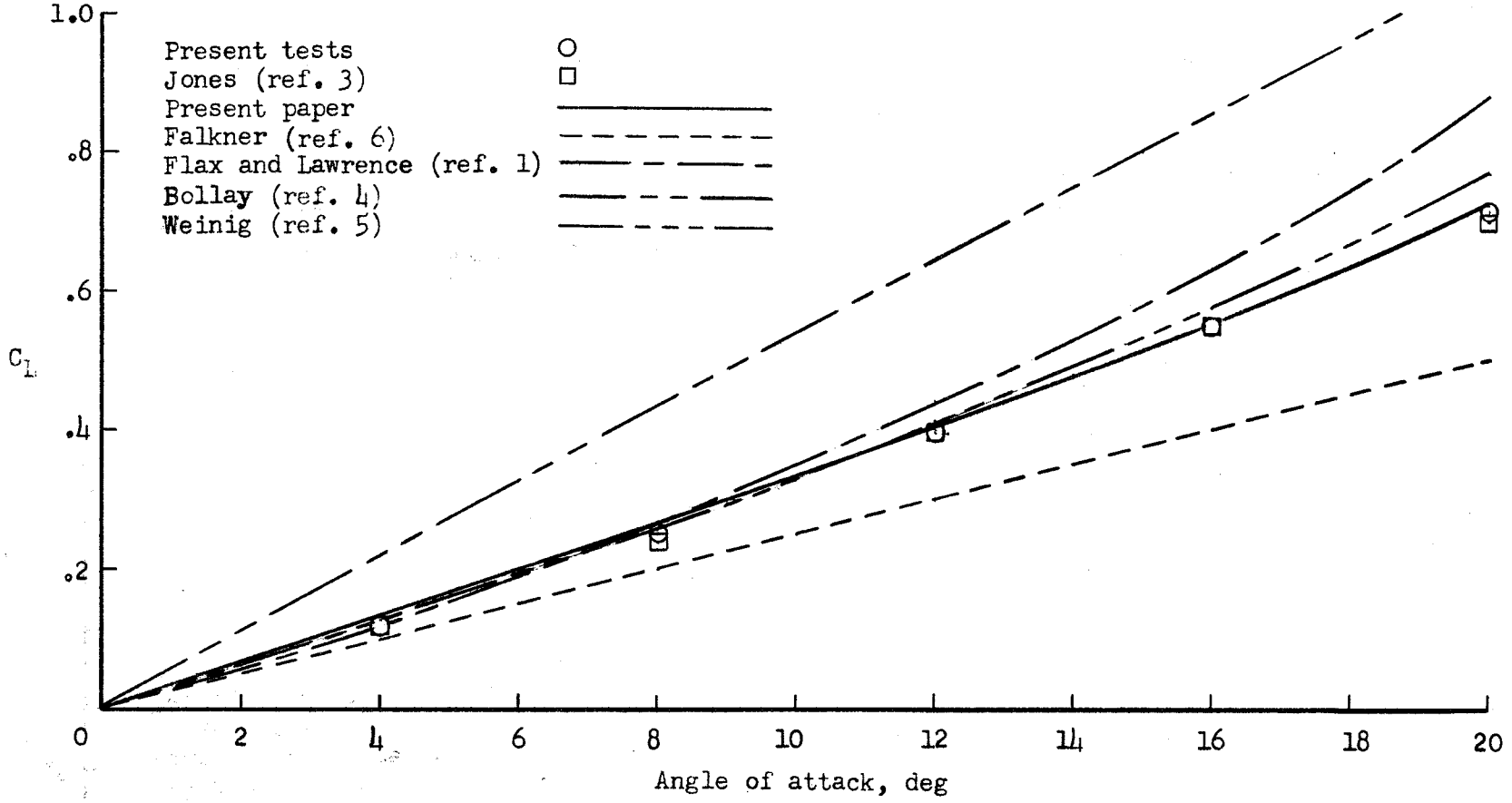

Figure 25.- Comparison between experimental and theoretical lift coefficients for aspect-ratio-1.00 surface.

NACA-Langley - 3-26-54 - 1000